NASA / CR-1999-209687

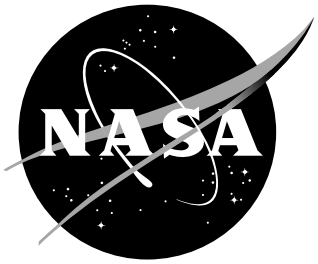

Broadband Transmission Loss Due to Reverberant Excitation

Lawrence P. Barisciano, Jr.
The George Washington University
Joint Institute for the Advancement of Flight Sciences
Langley Research Center, Hampton, Virginia

November 1999

The NASA STI Program Office ... in Profile

Since its founding, NASA has been dedicated to the advancement of aeronautics and space science. The NASA Scientific and Technical Information (STI) Program Office plays a key part in helping NASA maintain this important role.

The NASA STI Program Office is operated by Langley Research Center, the lead center for NASA's scientific and technical information. The NASA STI Program Office provides access to the NASA STI Database, the largest collection of aeronautical and space science STI in the world. The Program Office is also NASA's institutional mechanism for disseminating the results of its research and development activities. These results are published by NASA in the NASA STI Report Series, which includes the following report types:

- TECHNICAL PUBLICATION. Reports of completed research or a major significant phase of research that present the results of NASA programs and include extensive data or theoretical analysis. Includes compilations of significant scientific and technical data and information deemed to be of continuing reference value. NASA counterpart of peer-reviewed formal professional papers, but having less stringent limitations on manuscript length and extent of graphic presentations.
- TECHNICAL MEMORANDUM. Scientific and technical findings that are preliminary or of specialized interest, e.g., quick release reports, working papers, and bibliographies that contain minimal annotation. Does not contain extensive analysis.
- CONTRACTOR REPORT. Scientific and technical findings by NASA-sponsored contractors and grantees.
- CONFERENCE PUBLICATION. Collected papers from scientific and technical conferences, symposia, seminars, or other meetings sponsored or co-sponsored by NASA.
- SPECIAL PUBLICATION. Scientific, technical, or historical information from NASA programs, projects, and missions, often concerned with subjects having substantial public interest.
- TECHNICAL TRANSLATION. English-language translations of foreign scientific and technical material pertinent to NASA's mission.

Specialized services that complement the STI Program Office's diverse offerings include creating custom thesauri, building customized databases, organizing and publishing research results ... even providing videos.

For more information about the NASA STI Program Office, see the following:

- Access the NASA STI Program Home Page at *http://www.sti.nasa.gov*
- E-mail your question via the Internet to help@sti.nasa.gov
- Fax your question to the NASA STI Help Desk at (301) 621-0134
- Phone the NASA STI Help Desk at (301) 621-0390
- Write to:
  NASA STI Help Desk
  NASA Center for AeroSpace Information
  7121 Standard Drive
  Hanover, MD 21076-1320

NASA / CR-1999-209687

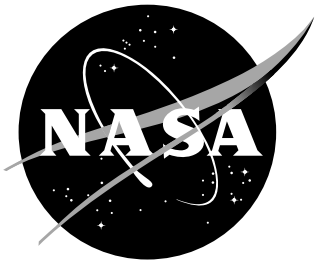

Broadband Transmission Loss Due to Reverberant Excitation

Lawrence P. Barisciano, Jr.
The George Washington University
Joint Institute for the Advancement of Flight Sciences
Langley Research Center, Hampton, Virginia

National Aeronautics and
Space Administration

Langley Research Center
Hampton, Virginia 23681-2199

Prepared for Langley Research Center
under Cooperative Agreement NCC1-14

November 1999

Available from:

NASA Center for AeroSpace Information (CASI)
7121 Standard Drive
Hanover, MD 21076-1320
(301) 621-0390

National Technical Information Service (NTIS)
5285 Port Royal Road
Springfield, VA 22161-2171
(703) 605-6000

Abstract

The noise transmission characteristics of candidate curved aircraft sidewall panel constructions is examined analytically using finite element models of the selected panel geometries. The models are validated by experimental modal analyses and transmission loss testing. The structural and acoustic response of the models are then examined when subjected to random or reverberant excitation, the simulation of which is also discussed. For a candidate curved honeycomb panel, the effect of add-on trim panel treatments is examined. Specifically, two different mounting configurations are discussed and their effect on the transmission loss of the panel is presented. This study finds that the add-on acoustical treatments do improve on the primary structures transmission loss characteristics, however, much more research is necessary to draw any valid conclusions about the optimal configuration for the maximum noise transmission loss. This paper describes several directions for the extension of this work.

List of Symbols

A	Area of an element, or region of influence for a nodal pressure
B_s	Structural damping matrix
C	Fluid-Structure coupling matrix
E	Young's Modulus
F	Applied force on structure
F_p	Force exerted by fluid on structure
G	Shear Modulus
H_{mn}	Transfer function
K_f,K_s	Fluid and structural stiffness matrices
M_f,M_s	Fluid and structural mass matrices
S_{ab}	Cross-correlation matrix
TL	Transmission loss
a,b	Indices of cross-correlation matrix
c	Speed of sound in air
i	$(-1)^{1/2}$
k	Wavenumber
m	Index of transfer matrix, referring to a "patch" of forces
n	Index of transfer matrix, referring to a data recovery node
p	Acoustic pressure
t	Laminate composite thickness
u	Structural displacement
r,t,z	Cylindrical coordinate system
x,y,z	Cartesian coordinate system
1,2,3	Material coordinate system
Φ_f,Φ_s	Uncoupled fluid and structure eignvectors
Π_{ref}	Incident acoustic power, or reference acoustic power
Π_{trans}	Total radiated acoustic power
α	Coefficient of thermal expansion
ν	Poisson's ratio
ξ_f,ξ_s	Fluid and structure modal amplitudes
ρ,ρ_f	Density of the fluid
ω	Frequency

CONTENTS

Abstract.....i

List of Symbols.....ii

Chapter 1 Introduction.....1

Chapter 2 Development of Model and Method, Preliminary Calculations, and Validation.....5
Section 1 Developing a Finite Element Model for a Sandwich Panel.....5
Section 2 Basic Methodology for the Calculation of Transmission Loss.....7
Section 3 Analysis of the Flat Sandwich Panel with Isotropic Core.....12
Section 4 Analysis of the Flat Honeycomb Panel.....15
Section 5 Modeling Random or Reverberant Excitation.....16

Chapter 3 Candidate Curved Sidewall Panel.....19
Section 1 Development of Finite Element Model.....19
Section 2 Model Validation.....22
Part 1 Normal Modes Analysis.....23
Part 2 Transmission Loss Analysis.....23
Section 3 Modeling of Add-On Treatment.....29
Section 4 Study of Trim Panel Mounting Configuration.....32

Chapter 4 Conclusions.....36
Section 1 Discussion of Results.....36
Section 2 Possible Improvements and Future Work.....37

Bibliography.....39

Appendix A Equations of Motion for a Frequency Response Analysis.....42

Appendix B Figures.....44

Appendix C Tables.....79

Appendix D FORTRAN Codes.....86

1. Introduction

Excessive in-flight aircraft interior cabin noise has long been a problem of study in structural acoustics. As new, faster civil transport planes continue to develop, this problem can only be expected to worsen as turbulent boundary layer noise becomes a larger contributing factor to these unacceptable noise levels [1]. It is for this reason that extensive research is being done in the High Speed Research Program on passive noise control techniques to lower the sound level inside the fuselage of high speed supersonic aircraft.

This study examines the problem of noise transmission through candidate curved aircraft sidewall panels. Specifically, the effect of add-on trim panels is of interest. The objective of this part of the High Speed Research Program is to perform a parametric study to determine the influence of several key parameters, involving the trim panels, on the panel's transmission loss characteristics for frequencies up to about 500 Hz. This frequency range was selected to ensure the accuracy and applicability of using the finite element method to study the panel, considering the panel size and geometry, and reasonable mesh densities. As stated earlier, turbulent boundary layer excitation is the main noise source of interest for the air flows which will be present in the flight conditions of these airplanes. As a first approximation, this study looks at random or reverberant excitation of the panel, which may be simulated in laboratory tests [2]. Also, reverberant excitation is studied because it is easier to model, and can be an excellent learning tool in beginning to model boundary layer excitation. Ultimately, this research hopes to deliver recommendations, regarding the appropriate trim and mounting

configuration, which help to significantly increase the noise transmission loss of the panel for the excitations of interest.

It must be noted that the High Speed Research program is also interested in studying the effect of other add-on acoustical treatments, such as fiberglass acoustical blankets and cap strips. Due to the limitations of time and available software, this is not addressed in this particular study. However, the work done here can serve as a foundation for this type of analysis.

This issue of noise transmission through aircraft panels, as well as the noise control benefits of acoustical treatments and trim panels, has been examined in many theoretical and experimental studies. Grosveld and Mixson looked into the noise control benefits of using acoustically treated and honeycomb stiffened aircraft sidewall panels [3]. They found that using a honeycomb core to stiffen the skin panels of an aircraft sidewall does increase the transmission loss. They also studied several different configurations of acoustic blankets and trim panels, comparing and contrasting the effects on the panels transmission loss characteristics. The subject of sound transmission through sandwich shells, in which a honeycomb core was sandwiched between composite face sheets was studied by Tang et al [4, 5]. They came up with an explicit expression for transmission loss through a cylindrical sandwich shell in terms of modal impedance of the fluids and the shell. They made comparisons of the transmission loss among various shell configurations, for different boundary layer source models. Some background research was also done to learn about the fiberglass acoustical treatments, mentioned earlier but not analyzed in this study. Bolton et al [6-8] extensively studied the use of elastic-porous materials, such as foam and fiberglass, in noise control applications. In

addition to studying ways to model these materials, they found that the noise transmission and absorption properties are highly dependent on the boundary conditions between the treatment and the primary structure. The acoustical characteristics of porous materials have also been studied by Attenborough [9]. He discusses the propagation of sound waves in porous media and also examines methods of determining the material properties of these media.

The present study is a theoretical look at the transmission loss characteristics of a curved sidewall panel, with laminated composite face sheets, stiffened by a honeycomb core. The proposed acoustic treatment materials are porous materials. Thus, the previously cited research efforts provide a basis and background for this work. Computational results are obtained using the commercially available analysis software: MSC/NASTRAN, COMET/SAFE and COMET/Acoustics. These results are validated and supported by experimentally obtained data for the panels of interest. Predictions and recommendations are made using the computational results, which model several variations on the lay-up of the built-up structure.

This study has been divided into two parts. In Chapter 2, some background material and the method of calculating transmission loss is laid out. This chapter also discusses a preliminary study performed on two comparable flat sandwich panels. At the close of the chapter, the discussion turns to the issue of modeling the random or reverberant excitation. Once all this background has been discussed, Chapter 3 examines the actual problem of the curved sidewall panel. Conclusions are drawn and recommendations for extensions of this work are made in Chapter 4. Appendix A describes the equations of motion for a frequency response analysis. Appendices B and C

contain the figures and tables, respectively. Finally, Appendix D contains the FORTRAN codes written to perform several calculations throughout this research.

2. Development of Model and Method, Preliminary Calculations, and Validation

Before it is possible to study the transmission loss characteristics of a trimmed curved sidewall panel, it is necessary to lay out and develop the method of calculating the transmission loss. Even more fundamental than that, though, it is essential to create a valid finite element model for the panel of study. This process involves using several commercial computer analysis programs as well as external FORTRAN codes.

A flat composite sandwich panel with an isotropic core, and a similar sandwich panel, but with a honeycomb core, were used as "test panels" in the development of this methodology. All of the analysis in this chapter was performed using these flat panel geometries.

2.1: Developing a Finite Element Model for a Sandwich Panel

The finite element method is employed in this research for determining the motion of the panel, subject to the excitations of interest. The finite element model is developed in MSC/PATRAN, a pre- and post-processing software package for MSC/NASTRAN, which is used to perform the finite element analysis.

The particular details of the sidewall panels of interest, and their finite element models will be discussed later. However, it is appropriate here to take a general look at the modeling choices and assumptions made in the development of a model for a sandwich panel with laminated composite face sheets. Two flat panel lay-ups were studied. The first was a homogenous, isotropic solid core sandwiched between the composite face sheets. The second used the same face sheets, but integrated with a honeycomb core. The lay-up for the honeycomb core is shown in Figure 1. The lay-up

for the first panel is similar, the only difference being that the core is solid and homogeneous.

The core is modeled using eight-node isoparametric hexagonal elements, or CHEXA elements as they are known within MSC/NASTRAN. These elements connect only translational degrees of freedom. Thus the nodes which comprise the element can only translate spatially, relative to each other. These elements can be given either isotropic or anisotropic material properties. The isotropic core references a MAT1 material bulk data card in the MSC/NASTRAN bulk data file. The honeycomb core can be modeled as an anisotropic material, and thus, the elements reference a MAT9 bulk data card. The MSC/NASTRAN documentation contains extensive background material on these elements' properties, as well as other elements used in this study [10-11].

The face sheets are modeled with four-node isoparametric elements or CQUAD4 elements. These elements obey the classical assumptions of thin plate theory. Nodes in these elements exhibit both translational and rotational degrees of freedom. In this study, the face sheets are laminated composites, in which each ply is a generally orthotropic material. Thus the CQUAD4 elements reference a laminated composite material, which is described in a PCOMP bulk data card. This PCOMP card, in turn, references the material properties of the individual plies, which are described in MAT8 bulk data cards.

In the model of the sandwich panel, the two face sheet elements, one on each side of the panel, are coincident with two faces of each of the hexagonal solid elements. Thus, the solid core and plate face sheet elements share nodes, i.e. they are equivalenced. This, therefore constrains the nodes of the plate elements so that they cannot rotate or translate independently of the nodes in the solid elements. This assumption is valid if the face

sheet is rigidly bonded to the core. The plate elements have a neutral axis offset automatically built into their laminated composite material properties which shifts the elements away from the solid elements by half the thickness of the composite.

A possible alternative for modeling the sandwich panel would be to actually physically offset the plate nodes from the solid nodes by half the laminate thickness. Each node could then be connected to the corresponding solid node by a rigid body element, or RBE2 element in MSC/NASTRAN, which constrains the displacements of the nodes but allows the plate nodes to have rotational degrees of freedom independent of the solid nodes. This method does not seem valid, though, if the face sheet is, in fact, rigidly bonded to the core, and therefore is not considered in this study.

Once the elements have been created, the remaining tasks in the development of the model are to assign boundary conditions and element properties. This can all be done within MSC/PATRAN. Once the model is created, a bulk data file is written which serves as input for a finite element analysis in MSC/NASTRAN.

2.2: Basic Methodology for the Calculation of Transmission Loss

Before beginning a discussion of the methodology, it is worth mentioning here exactly how transmission loss has been defined, since this is often a somewhat vague term. In this study, transmission loss has been defined as

$$TL = 10 * \log(\frac{\Pi_{ref}}{\Pi_{trans}}) \qquad \textbf{(1)}$$

The reference power, Π_{ref}, is the acoustic power of the incident sound field. The acoustic power of the transmitted sound field, Π_{trans}, is the total radiated power in the far field.

The first step in computing the transmission loss of a panel, once a valid finite element model of the panel has been developed, is to determine the panel's vibration response. This is accomplished using MSC/NASTRAN to perform a frequency response analysis. See Appendix A for a description of the equations of motion for a frequency response analysis. In order to simulate a particular excitation, the incident side of the panel is divided into arbitrarily small regions which from this point on will be referred to as "patches." These patches are groups of nodes, within which each node is forced with a unit harmonic force, oriented normal to the face of the panel. The forcing at each particular node in the patch is in phase with every other node in the patch. However the forcing at each patch is totally uncorrelated with the forcing at every other patch. Thus, if one wanted to model a normally incident plane wave, one patch over the incident side of the panel would be correct. If one wanted to simulate random incidence, each node on the incident side would be one patch, in itself. This is further discussed in Section 2.5. A frequency response analysis, using the modal method (SOL 111), is performed in MSC/NASTRAN to determine the velocities at each node on the response side of the panel, given the forcing at each individual patch. Thus there would be one analysis for each forcing at each patch at each frequency of interest. Figure 2 shows the hierarchy of bulk data cards which must be included in the bulk data file to model this type of excitation.

Note that this same procedure could be applied to a built up panel using COMET/SAFE (SAFE stands for Structural Acoustic Foam Engineering) instead of MSC/NASTRAN. The reason for using a different analysis code is the capability of COMET/SAFE to handle elastic-porous foam elements, which can be used to model

acoustic blankets and cap strips. The disadvantage of COMET/SAFE, however, is its inability to model any structural (solid) materials which are not isotropic. Thus, it cannot accurately model the laminated composite face sheets or the honeycomb core of the flat honeycomb sandwich panel or the curved honeycomb sandwich panel which are studied in this research. Also, COMET/SAFE has excessively long run times for cases in which the excitation requires many patches. For these reasons, the current version of COMET/SAFE is not used in this study.

The velocities generated by the frequency response analysis must be written to a "punch" file, which is basically a results file written in a format readable by other programs. This results file, along with the MSC/NASTRAN bulk data file for the model, is used to perform a direct boundary element analysis in COMET/Acoustics to determine the acoustic radiation transfer functions.

Using COMET/Vision, which is a pre- and post-processor for COMET/Acoustics, one can import a boundary element mesh created in MSC/PATRAN. In this case, the boundary element mesh would be a "box" which has five hard walls and one elastic wall, which represents the response side face sheet of the panel. Thus, one can think of the boundary element mesh as a "source room," and the region exterior to this room as the "receiving room" in a transmission loss test. The boundary element mesh used for the flat sandwich panel is shown in Figure 3. The direct boundary element method is very convenient in this case because it solves for acoustic pressure and velocity in either the interior or exterior regions. The panel velocities, determined by MSC/NASTRAN, can be imported and used as velocity boundary conditions for those elements and nodes of the boundary element mesh corresponding to the response side of the panel. A spherical data

recovery mesh in the far field is used to determine the acoustic pressures for the sound field radiated by the panel. The data recovery mesh is shown in Figure 4. A direct boundary element analysis, performed for the exterior region of the box, yields the acoustic radiated pressure due to the forcing function at each patch, for each frequency.

Once all the acoustic pressures have been calculated, the results file generated by COMET/Acoustics is used as an input file to the external FORTRAN code, response.f, which computes the transfer matrix H_{mn} and power spectral density of the panel $H_{mn}{}^{T}S_{ab}H_{mn}{}^{*}$ at each frequency. See Appendix D for a discussion of all external computer codes used in this study.

The transfer matrix, which describes the acoustic radiation of the panel as measured at the far-field data recovery nodes, for harmonic loading at each patch for each frequency, is an m by n matrix, where m is the number of patches and n is the number of data recovery nodes in the far field. S_{ab} represents the cross-spectral loading, which in this case will either model plane wave or reverberant excitation. The cross spectral loading matrix is an m by m matrix. Since random excitation is the incident field of choice in this study, the cross spectral loading matrix is a diagonal matrix. Each diagonal entry is unity. This implies that the panel response due to forcing by each uncorrelated patch is scaled equally.

The power spectral density is used to calculate the transmission loss at each frequency according to Equation (1). The reference power, Π_{ref}, must be determined accordingly for the particular excitation. This is dependent upon the number of patches. For example, if the incident side of the panel, which in initial modeling attempts had a 12 x 12 element mesh and 169 nodes, is all one patch, then the total force applied to the

panel would be 169 N. If the panel, with the same mesh, is divided into four patches, then each patch will have 49 nodes (assuming that the nodes located on adjacent sides of the patches are included in both patches), and thus 49 N of force. The input acoustic power for these two cases would be determined by calculating the pressure at each node, integrating it over the surface of the incident side of the panel, and using the following approximate equation:

$$\Pi_{ref} = \frac{A(pp^*)}{2\rho c} \qquad \textbf{(2)}$$

where A is the "area of influence" of the node in the data recovery mesh. It is basically the area over which the acoustic pressure acts. Note that this equation is only truly valid for a free acoustic field. It is only an approximation for this case.

An alternative, simpler approach for determining the input power would be to simply define the input power to be the sum of the input forces squared. Thus, for the one patch case, the input "power" would be $(169)^2$ N^2. This one patch case is the case by which all other excitations will be normalized. Thus, this input power will be defined to be one unit of power. For the four patch case, the input power would be $4*(49)^2$ N^2 which, relative to the one patch case, is .3363 units of power. In general, the input or reference power is

$$\Pi_{ref} = \frac{\sum_{1}^{\#ofpatches} \left(\sum_{1}^{\#nodes/patch} 1 \right)^2}{(Total\#ofnodes)^2} \qquad \textbf{(3)}$$

where the "total number of nodes" refers to the total number of nodes on the incident side of the panel, which is 169 in the case of the 12x12 element mesh. This would not give the actual transmission loss, but rather a relative transmission loss. It will be seen in later

sections of this chapter that this idea of relative transmission loss proves to be quite useful.

In future cases, the cross-spectral loading matrix will be used to model turbulent boundary layer excitation. For this type of excitation, the forcing at each patch is correlated in some way to the forcing at adjacent patches. This is accounted for in the cross-spectral loading matrix by the presence of non-zero off-diagonal terms. There is ample discussion of turbulent boundary layer modeling methods in the literature [13-17].

2.3: Analysis of the Flat Sandwich Panel with Isotropic Core

Although the primary focus of this research is to study the transmission loss characteristics of candidate curved sidewall panels, an initial study was performed on two flat sandwich panels. The flat panel is a desirable learning tool because of its relatively simple geometry, yet it has lay-up properties similar to the curved panel of interest.

The first flat panel was a sandwich panel with an isotropic core sandwiched between two laminated composite face sheets. This panel was actually studied by accident. As a first modeling attempt, the core of the panel, which was supposed to be titanium honeycomb, was incorrectly modeled as an isotropic material. Although this panel lay-up does not correspond to the actual panel studied by the High Speed Research Program, the results shown in this section and the conclusions drawn are still applicable to the honeycomb panels studied later.

This particular panel has planar dimensions of 36” x 36”. It has a 1” thick Ti3Al2.5V solid, homogeneous, isotropic core sandwiched between two laminated composite face sheets. The layers of the laminated composite are IM7/PETI5. The panel

is assumed to have 5% structural damping. Table 1 details the properties of the component material of the panel.

A finite element model of this flat isotropic-core panel was developed in MSC/PATRAN, as shown in Figure 5. Initially, a 12x12 element mesh of CQUAD4 plate elements was selected for each of the face sheets, while a 12x12 element mesh of CHEXA brick elements, one layer thick, was selected for the core.

A normal mode analysis was performed in MSC/NASTRAN. The edges of the panel were clamped for this analysis. The results of the normal mode analysis are used to verify the resonance frequencies of the panel, with clamped boundary conditions. These results are shown in Table 2. When the transmission loss of the panel is studied as a function of frequency, a minimum in the curve of transmission loss vs. frequency typically indicates that a panel mode occurs at that particular frequency. This is due to the more significant panel response at a resonance, and thus the larger acoustic pressure of the radiated acoustic field.

In order to validate this model, several basic checks were performed. First, it was verified that the model obeys the Mass Law of Sound in the mass-controlled frequency region. The Mass Law of Sound states that there is a 6dB increase in transmission loss per octave in the mass-controlled region, which is the frequency region above the panel resonances but below coincidence. The panel was divided into four patches, in which each patch contains 49 nodes and thus 49 N of force. As stated earlier, the input power in this case is .3363 units. The relative transmission loss as a function of frequency was calculated as described in the previous section. Figure 6 shows that the curve has a

6dB/Octave slope in the mass controlled region, which lies in the frequency range above 375 Hz.

Another study performed to check the validity of the finite element model was an in-depth look at the transmission loss vs. frequency characteristics of the panel in a small range of frequencies around the first panel resonance, which is the (1,1) mode. This analysis was run for one patch, or a normal incidence plane wave, with no structural damping in the model. Considering the mode shape of the (1,1) mode, one would expect that a normal incidence plane wave would greatly excite this mode. Thus, the transmission loss should vanish at the first resonance frequency of the panel, since nearly all of the sound would be transmitted. This is demonstrated in Figure 7.

The final step in the development of the finite element model is to determine the necessary mesh density to obtain a converged solution. As stated earlier, a 12x12 element mesh density was initially used. This mesh was made finer by increasing to a 14x14 element mesh, and made coarser by decreasing to a 9x9 element mesh. The main concern in this study was the ability of the chosen mesh density to accurately reflect the high order modes of the panel. Since the excitation of all the panel modes of vibration is necessary for this part of the study, each individual node on the incident side if the panel was treated as a patch and forced independently. However, to keep the input power constant, the force applied to each node on the incident side of the panel, for the coarse and fine meshes, was adjusted so as to have 169 N of total force applied to the panel. Thus, the input power was 169 N^2 or .0059 units of power relative to the one patch case for the 12 x12 element mesh. The results of this study are shown in Figure 8. The results indicate that 12x12 element mesh density is sufficient to obtain a solution which, although it is a

few decibels below the finer mesh solution, accurately captures all the higher order panel modes.

2.4: Analysis of the Flat Honeycomb Panel

The flat honeycomb panel, panel 261X1423-20, was developed for study in the High Speed Research Program. The panel, shown in Figure 9, like the isotropic-core panel, has in-plane dimensions of 36" x 36" with a 1" thick core. The component materials are also the same. Once again, 5% structural damping is assumed. The difference for this panel is that the core is honeycomb, and is thus modeled as an anisotropic material. The specific material properties of the core are shown in Table 3. It should be noted that some of these material properties for the core were measured directly, and those which were not were determined from the intrinsic material properties of Ti3Al2.5V, which are shown in Table 1 [4].

The finite element model for this panel looks the same as for the previous model, which was shown in Figure 5. The only difference is the designation of new material properties for the core. Once again, a normal mode analysis was performed in MSC/NASTRAN for the panel. This time, though, it was performed for two boundary condition configurations. The first was a "free-free" configuration. This set-up mirrors an experimental modal analysis, which was performed on the panel at NASA Langley Research Center at the Thermal Acoustic Fatigue Apparatus (TAFA) Facility. The frequency response of the panel at various reference points due to a "tap" impulse was measured using accelerometers. The polyreference curve-fitting technique was used to determine the mode shapes of the panel and their associated frequencies [20]. The results of this experimental modal analysis have been used to validate the modes of the panel

predicted by the finite element model, as shown in Table 4. The second boundary condition configuration was one in which the edges of the panel were clamped. This situation simulates the panel's experimental transmission loss testing configuration by the Boeing Company under the High Speed Research Program. Table 5 shows the results of the modal analysis with clamped edge boundary conditions.

It should be noted that the frequencies shown in Table 5 for the clamped flat honeycomb panel were significantly higher than the ones shown in Table 2 for the isotropic-core panel. In fact, there is only one panel resonance within the frequency range 0-500 Hz, which is the range of interest in this study. Thus, in any relative transmission loss vs. frequency curves for this panel there will only be one minimum, and the transmission loss characteristics of the higher order modes of the panel will not be displayed. It is for this reason that the previous panel's results are so important. Without them, the conclusions about finite element modal mesh density and model validation according to the Mass Law of Sound could not be clearly drawn.

For completeness, though, Figure 10 shows the relative transmission loss vs. frequency curves for the same mesh densities as for the isotropic-core panel. This plot shows a small frequency range around the first panel resonance because of the extensive computation time involved with performing this analysis for individual nodal forcing.

2.5: Modeling Random or Reverberant Excitation

Reverberant excitation describes a sound field in which the sound level is constant but there is random phasing [18]. Basically, it is a random incidence sound field, in which the excitation at every point on the incident side of the panel is totally uncorrelated with that at every other point. Reverberant excitation is of interest because a reverberant

acoustic field is the standard forcing function employed in transmission loss testing. It is also of interest because it is relatively easy to model, while still allowing for adequate excitation of the higher order modes of the panel.

An accurate and reliable simulation of reverberant excitation is highly dependent on the number of totally uncorrelated forces or patches, which are incident on the panel. Since the sound level in a reverberant field is constant, the cross spectral loading matrix S_{ab} is once again represented by a diagonal matrix in which each diagonal entry has the nominal value of unity.

It is necessary to determine the required discretization of patches or forces required to adequately simulate reverberant excitation. A study was performed on both of the flat sandwich panels, which were previously discussed, to determine the appropriate number of patches. This study began, for each panel, by determining the relative transmission loss as a function of frequency for one patch, which corresponds to a totally correlated force, or a normal incidence plane wave, over the face of the panel. The forcing was then modified by subdividing the incident side of the panel into increasing numbers of patches to see how this affected the relative transmission loss characteristics of the panels where once again all the input power values were normalized by the one patch case. The results for the isotropic core and honeycomb core panels are shown in Figure 11 and Figure 12, respectively. These figures show that as the number of patches is increased, the relative transmission loss vs. frequency curves converge. Figure 11 also suggests that the case in which each node is forced individually best excites the higher order even modes of the panel. Figure 13 shows the “power” spectra for a node on the response side of the isotropic core flat panel for the one patch and the individual nodal

forcing cases. This node, for which the panel response was calculated, was chosen such that it would not lie along any panel mode node lines or lines of symmetry. The chosen node was located three element lengths in the 'x' direction and four element lengths in the 'y' direction from the corner of the panel. Power at each frequency was calculated by multiplying the normal component of the velocity of the node by its complex conjugate, and summing this for every forcing case at that frequency. Figure 13 shows that the one patch case best excites the odd panel modes, but that the individual nodal forcing case excites all the modes, although weakly in comparison to the one patch case. One would expect that for increasing numbers of patches, the one patch curve would converge to the individual nodal forcing curve. Considering all three of these figures, one can conclude that in order to get an accurate model of the random excitation, which excites all the modes, each node on the incident side of the panel should have its own unit force, which is totally uncorrelated to the force at each other node.

There is one feature of these results which is puzzling at first glance. One would expect that for the first panel mode, which is the (1,1) mode, the normal incidence plane wave, or one patch case, which best excites this mode, would have the lowest transmission loss, despite the different input powers for the different numbers of patches. However, as evidenced by Figures 11 and 12, this did not happen. This can be accounted for by the difference in input power for the two forcing cases. The input power for the one patch case is 169 times greater than for the individual nodal forcing case, while the panel response is only approximately 33 times greater. Since the panel response is proportional to the radiated power, this would indicate that the individual nodal forcing case has better noise transmission and thus, less transmission loss.

3. Candidate Curved Sidewall Panel

As stated earlier, this research is mainly concerned with the transmission loss characteristics of curved aircraft sidewall panels. This chapter describes studies which were performed on a specific candidate curved sidewall panel, provided by the High Speed Research Program. First, there is a description of the finite element model for the panel and also the efforts to validate this model. Then the discussion turns to the add-on trim panels, how they affect the finite element model, and the transmission loss results.

3.1 Development of the Finite Element Model

The curved panel to be studied is a stiffened sandwich panel with a honeycomb core. The honeycomb core is made of Aluminum 5052, the properties of which are detailed in Table 6. The face sheets are laminated composite, eight plies thick, in which seven of the plies are BMS 8-212 Type III and the other ply is BMS 8-212 Type IV. Both of these ply materials are 2-D orthotropic materials. The material properties of these two materials are shown in Table 7. Table 8 shows the stacking sequence of the laminate. The stiffeners have an inverted "T" cross section. The web of the stiffeners is made of Aluminum 6061 and the flange is made of Aluminum 2024. The material properties of these two isotropic materials are given in Table 9.

There were no clear photographs of the panel available. Figures 14 and 15 show a full view and a side view, respectively, of the finite element model for the panel, respectively. Although, the details of the finite element model will be discussed later, these figures can also serve as a picture of the panel in order to understand the physical geometry. The panel is 2.49 meters by 1.77 meters where 1.77 meters is the length of the arc segment on the inside curvature from edge to edge. The outside curvature is 1.64

meters from the beginning of the tapered edge to the beginning of the other tapered edge. The core is .013 meters thick. The tapered edges are .032 meters in length and then there is a .032 meter lip. Figure 17 shows a cross-sectional view of the panel near an edge. Figure 18 shows a cross-sectional view of the stiffeners, and the corresponding dimensions. The webs of the stiffeners are located 1.02 meters apart along the longitudinal length of the panel, with the web of the center stiffener located at the longitudinal centerline. There is a mechanical fastener, which fastens the stiffener to the panel, every .0762 meters along the length of the stiffeners. The total weight of the panel is 97 pounds.

The finite element model for this panel is more complicated than for the earlier flat panels, mainly due to the curvature, the stiffeners, and the tapered edges. However, the basic modeling techniques described in Chapter 2, Section 1 are still applicable. This curved panel, like the flat panels, was modeled using CQUAD4 plate elements as the face sheets which "sandwich" the HEXA solid elements that constitute the core. Since the honeycomb core is modeled as an anisotropic material, the coordinate system governing each element must be consistent. A cylindrical coordinate system, with the origin at the center of curvature, at the longitudinal edge of the panel, proved to be most appropriate, considering the curvature of the panel. This coordinate system, as well as the global cartesian coordinate system for the model which shares the same origin, is shown in Figure 16. This is not a problem with the CQUAD4 elements because the local coordinate system for these elements, in MSC/NASTRAN, is such that the 1-2 principle material directions are always "in-plane."

Each of the three stiffeners is treated as two separate entities in the model: the web and the flange. The web is comprised of CQUAD4 plate elements, each of which is oriented normal to the face sheet elements, and reference a MAT1, isotropic material bulk data card. The flange, also made of an isotropic material, is treated a little differently. It is modeled as the top ply, ply #9 according to Table 8, in the laminated composite. Thus, the ply references a MAT1 isotropic material, but the CQUAD4 elements reference a laminated composite, or a PCOMP bulk data card. Therefore, the curved face sheets of the panel are comprised of two different types of laminated composite: that which is described in Table 8, and a composite in which the flange is the top ply where there is a stiffener.

After the edges have tapered, there is a .032 meter lip on each side of the panel. As shown in Figure 17, this lip, where the inside and outside face sheets come together, is twice the thickness of the laminated composite. Its ply lay-up is such that the eight plies in Table 8 are half of a symmetric 16 ply laminated composite.

The next step in the development of the finite element model is to create an appropriate mesh. It was found for flat panels in Chapter 2 that the element area of the CQUAD4 elements need not be less than .0058 square meters (for the 12x12 element mesh) , but must not be greater than .0103 square meters (for the 9x9 element mesh). Since the CQUAD4 elements at the flanges of the stiffeners have different material properties than the rest of the face sheets, the longitudinal length of these elements should be no longer than the longitudinal length of the flanges of the stiffeners. If this longitudinal length of the flanges is divided into two elements, which are .0635 meters in length (for ease of having an easily divisible number of nodes in the longitudinal

direction of the panel for subdivision into patches), and there are 23 elements of length .0714 meters in the circumferential, or transverse direction (motivated by the location of the mechanical fasteners on the stiffeners), then the area of each of these elements is .0043 square meters. If a uniform element mesh over the whole face sheet of the panel is used, then the elements will be smaller than necessary and the mesh will be too fine. However, the mesh is constrained by the need to have these smaller elements of a certain longitudinal length at the flanges of the stiffeners. A solution is to use a non-uniform mesh in the longitudinal direction. This mesh has elements which have the appropriate longitudinal length at the flanges, but a larger length of .127 meters longitudinally along the panel in between the stiffeners. If the element length in the lateral direction is kept the same, and uniform, this yields some elements with larger areas, but all are still within the limits set above, and thus it gives a suitable finite element mesh for the face sheets. Also, it should be noted that the length scales of these elements is consistent with the accepted "rule-of-thumb" that there should be at least five elements per wavelength of the highest order mode to be considered. As in the case of the flat panels, the core is modeled with one layer of eight-node hexagonal HEXA elements. The length and width of these elements matches the face sheet elements. The webs of the stiffeners have two CQUAD4 elements along the height. In the circumferential direction, there are 23 elements, which matches the face sheets in this direction.

3.2 Model Validation

There were two studies performed to validate the finite element model for the curved honeycomb panel. The first was a normal mode analysis to validate the dynamic

response of the panel. Then a transmission loss analysis was performed on the panel to validate the acoustic response.

3.2.1 Normal Mode Analysis

An experimental free-free modal analysis was performed on the curved honeycomb panel by the Boeing Company as part of the High Speed Research program. The free-free boundary condition set-up was achieved using bungee cords to support the panel along the transverse centerline of the panel. There were thirty-six accelerometer reference points at which the panel response was measured. The excitation was a "tap" impulse at a chosen reference point. There were several of these "tap reference points." The frequency response functions due to the various excitations were used in a polyreference curve-fitting, as for the flat honeycomb panel, to estimate the experimental mode shapes and frequencies.

These results were used to validate the finite element model. A modal analysis was performed in MSC/NASTRAN with free-free boundary conditions. The results are shown in Table 10. This table shows that the finite element model fairly accurately captures the dynamic response of the panel. A modal analysis was also performed on the curved panel, with the edge of the lips clamped. This is the boundary configuration for the panel when it is used in the Boeing Company's Transmission Loss Facility. These results are shown in Table 11.

3.2.2 Transmission Loss Analysis

The other attempt to validate the curved honeycomb panel finite element model was to study the transmission loss characteristics of the panel for comparison with experimentally obtained results. The Boeing Company performed a transmission loss test

in which the excitation was an obliquely incident acoustic plane wave, 30° from normal incidence, on the outside curved surface of the panel. This test was performed in the Boeing Company's Fuselage Sidewall Panel Transmission Loss Facility (FSPTLF). The panel was bolted, i.e. clamped, at the edges to secure it in the transmission loss facility window, which is 1.12 meters by 1.73 meters in size. Special "transition filler walls" were constructed to fill in the gap in the wall due to the size and curvature of the panel. Figure 19 shows a diagram of the FSPTLF. The low frequency cut-off is around 100 Hz for the semi-anechoic chamber configuration. Figure 20 shows some details of the mounting configuration for the test. It should be noted that the test engineers who performed the test realized that the excitation was not actually an oblique incidence plane wave because of reflections in the source room.

A transmission loss analysis was performed on the finite element model for the curved honeycomb panel. The first step in performing this analysis was to model the excitation. As stated earlier, the incident field was intended to be a plane wave which is incident on the panel at an angle of 30° from the normal along the transverse centerline of the panel. COMET/Acoustics was used to calculate the pressures on each element of the incident side of the panel assuming a plane wave source. The incident side of the panel is treated as a blocked panel or a rigid surface for this part of the analysis, since the concern here is to model the excitation and not to calculate the panel's response [19]. Thus, the magnitude and phase of the pressure on the incident side of the panel varies with position and frequency. To calculate this pressure variation in COMET/Acoustics, one must create a boundary element mesh. In this case, the boundary element mesh should somewhat resemble the receiving room of the transmission loss facility. A mesh,

identical to the incident side of the panel, is placed in the center of a large flat baffle. There must be five rigid sides around the baffle, to create a “box” or a “room”. This is to isolate the back of the panel. If this is not done, the pressures on the back of the panel due to the plane wave source will affect the results and not give a true picture of the pressure field on the incident side of the panel. For this analysis, only the acoustic field in the exterior region of the box is of interest. A plane wave source is placed in space, outside the box, and directed such that it impinges on the boundary element mesh at the appropriate angle. This set-up somewhat mirrors the experimental set-up. The main difference is that the source is located out in space, approximately six and half meters away from the panel, as opposed to being confined in a source room. Thus, the theoretical model does not account for reflections of the sound field off the other five walls of the source room in the transmission loss facility. The magnitude of the acoustic pressure of the source was one Pascal. The boundary element mesh and source are shown in Figures 21 and 22. A direct boundary element analysis in the exterior region of the mesh was performed in COMET/Acoustics over the frequency range 5 - 505 Hz. Figure 23 shows the magnitude of the acoustic pressures on the boundary element mesh for a sample frequency of 205 Hz. Figure 24 shows the phase of the acoustic pressures for the same frequency.

At first, the results shown in Figure 23 were a bit puzzling. One would expect that for a plane wave for which the direction has an x and a z component, that the magnitude of the pressure along the transverse centerline of the panel would be nearly constant because the incident and reflected waves along this centerline should be the same all along it. This is not the case, though. To try to resolve this, the same analysis

was run for a plane wave, directed normal to the transverse centerline of the panel. One would fully expect that there would be only very slight variation in pressure magnitude along the transverse centerline of the panel for this case. Figure 25 confirms this, but shows that there are slight variations of the pressure magnitude near the edges. This would lead one to believe that these edge effects are simply more pronounced for the oblique incidence plane wave. As a final confirmation of the edge effects of the boundary element mesh, the analysis was run for a normal incidence plane wave on a boundary element mesh in which the curved panel was removed from the baffle, leaving a large flat rigid wall on the front face. The results are shown in Figure 26. This figure shows that the pressure magnitude is nearly constant except near the edges, as expected. Thus, it can be concluded that although the pressure magnitude results for the oblique plane wave seem counter-intuitive, they are reliable, and the discrepancies are due to effects of the edges in the boundary element mesh.

COMET/Acoustics can be set such that it calculates the acoustic pressures on each element in the boundary element mesh. An external Fortran code, comet2nastran.f, was written to read the COMET/Acoustics element results file, pick out the pressures on each element on the incident side of the panel, and write this information in a MSC/NASTRAN bulk data format. This code is given in Appendix D. Thus, a bulk data file can be set up to perform a frequency response analysis in MSC/NASTRAN for an obliquely incident acoustic plane wave, with an acoustic pressure magnitude of one Pascal , to determine the velocities of the nodes on the receiving side of the panel, for which the nodes of the edge of the lip are clamped. Rather than applying dynamic forces to each node of the incident side of the panel, as for the flat panel cases described in

Chapter 2, this analysis requires that dynamic pressures be applied to each element of the incident side of the panel. This is accomplished with the PLOAD4 bulk data card in MSC/NASTRAN. Figure 27 shows the hierarchy of MSC/NASTRAN bulk data cards which must be included in the bulk data file to simulate the desired excitation. Although every element has a different magnitude and phase of pressure, there is only one analysis per frequency, in which every element is given the appropriate pressure. This is in contrast to the random incidence case in which each node is forced separately in its own analysis for each frequency, which was described in Chapter 2.

The results of the frequency response analysis, i.e. the velocities on the response side of the panel, are imported as velocity boundary conditions for an acoustic analysis in COMET/Acoustics. The boundary element mesh for this case is similar to the one used for the flat panels in Chapter 2, except that the elastic wall in this case has the curvature of the response side of the panel. The other five rigid walls are flat, as in the previous cases. The boundary element mesh is shown in Figure 28. A spherical data recovery mesh in the far-field, identical to the one used in the flat panel cases as shown in Figure 4, once again calculates the acoustic pressures due to the radiated sound field. Response.f, the same external Fortran code as before, uses the results from COMET/Acoustics to build the transfer matrix, compute the acoustic response of the panel, and calculate the transmission loss at each frequency. Note that the code must be modified slightly such that the transmission loss is calculated with a reference power which reflects the actual acoustic power of the incident sound field. For a plane wave, the acoustic power is given by

$$p = Ce^{-ikx}$$
$$C = 1Pascal \qquad \textbf{(4)}$$
$$\Pi_{ref} = \frac{1}{2}\mathrm{Re}(pv^{*}) = \frac{1}{2}\mathrm{Re}(\frac{pp^{*}}{\rho c}) = \frac{1}{2\rho c} = .0012Watts$$

The transmission loss vs. frequency results for both this theoretical case and the experiment described earlier are shown in Figure 29.

Note that Figure 29 shows three theoretical curves. These three cases represent three different structural damping cases. In all previous analyses, the panels were assumed to have 5% structural damping. This is a reasonable first guess for the panels considered in this study. However, it is just a guess. A slightly higher and slightly lower value of 7% and 3%, respectively, were studied in hopes of better correlation with the experimental results. The three curves show a lower transmission loss than the experimental results for frequencies above 200 Hz, which marks the beginning of the damping controlled frequency region. It is this frequency region that the theoretical analysis hopes to match the experimental results. Below this frequency, in the stiffness controlled frequency region, the experimental results are not as reliable because the frequencies are close to the low frequency cut-off for the transmission loss facility. Though the magnitude of transmission loss is off in the damping controlled region, the theoretical curves show some of the same trends as the experimental curve for several panel modes. This leads one to believe that the finite element model for the curved honeycomb panel gives a fairly good approximation of the panel's acoustic response, assuming that the experimental results are correct. The discrepancies in this frequency region are most likely due to two factors. First, the mounting of the panel for the experiment, as shown in Figure 20, indicates that the panel may have been clamped at

more than just the lips at the edge. Second, as stated earlier, in the experiment the incident field was not a true plane wave due to reflections off the walls of the source room. This was not accounted for in the theoretical analysis. As for the proper percentage of structural damping, it appears that the 7% damping case loses most of the modal characteristics in the damping controlled region. Thus, it is concluded that 5% structural damping is sufficient to model this curved honeycomb panel.

3.3 Modeling of Add-On Treatments

The trim panel used in all High Speed Research Program Transmission Loss testing is a cargo liner which conforms to Boeing Material Specification 8-223, Grade B, Class 2, Type 50. The material properties are given in Table 12. Figure 30 shows a photograph of the trim panels used for the curved honeycomb panel before attachment. Figure 31 shows a photograph of the set-up with the trim panel attached to the bare panel. The green "sides" attached to the trim panel in this photograph are clay, which was used to mount the trim panels in the experimental transmission loss set-up.

Adding the trim panels to the finite element model for the curved honeycomb panel proved to be challenging. The cargo liner material was modeled as an isotropic material using CQUAD4 elements. In the model, the trim panels were assumed to have the same curvature as the bare panel structure and are offset from the inside curved surface of the panel by the height of the webs of the stiffeners. The transverse edges of the trim panels are coincident with the edges of the webs of the stiffeners. Thus, the trim panels only covered the inner two bays of the panel. The edges of the trim panels and webs are coincident, but the nodes along these two edges are not equivalenced. Doing so would clamp these two edges together. As will be discussed later, the method of

mounting the trim panel to the bare panel construction is a key parameter of study. For different mounting configurations, certain edge nodes of the trim panels and webs could be attached with rigid body constraints. The modeling of the air gaps, which are represented by solid CHEXA elements, in between the bare panel surface and the trim panel within each bay was the difficult part. Figure 32 shows the finite element model for the built-up panel. Note that the small circles represent RBE2 rigid body elements, which are used to connect the trim panel to the webs of the stiffeners. In this figure, the corners of the trim panel are pinned to the webs.

Since the interaction of the air in the air gaps and the structure is critical to the noise transmission characteristics of this built-up panel, it is necessary to exploit the fluid-structure coupling capabilities of MSC/NASTRAN. Fernholz and Robinson did an extensive study in this area outlining the procedures and methods for performing such an analysis [21]. This paper will not restate all of their findings, but rather it will touch on aspects of the fluid-structure coupling which are unique to this finite element model.

In order to couple the fluid and structure, the fluid-structure interface must be defined in the MSC/NASTRAN bulk data file. The computationally efficient way to do this is to create coincident fluid and structural nodes along the interface. These nodes should not be equivalenced, so that two nodes are left at every grid point in the interface. The fluid-structure interface is then specified in the bulk data file by listing the fluid nodes and the structural nodes which lie on the interface. The ACMODL bulk data card defines the modeling parameters for the interface. If the type of interface indicated in this card is “IDENT”, MSC/NASTRAN will find the corresponding and coincident fluid and structural nodes on the interface from the list of such nodes which was specified already.

The difficulty occurs for the grid points along the transverse edges of the trim panels and webs. Since these structural edges are supposed to be coincident, but not equivalenced (due to structural mounting considerations), there are two structural grid points at each of these points for the outer two stiffeners, and three structural grid points at each point along the center stiffener web, which are supposed to correspond to one fluid grid point. MSC/NASTRAN cannot perform the coupled analysis for such an interface.

To remedy this situation, it is necessary to create some fluid "filler" elements, as shown in Figure 33. These filler elements are thin 3-D fluid elements. These elements provide enough fluid grid points at the fluid-structure interface to have a one-to-one correspondence between the fluid grid points and the structural grid points. It should be noted that the edges of the trim panels are now slightly offset from the edges of the webs (by the width of the filler elements), but, as stated earlier, RBE2 rigid body elements can be used to attach the trim panels to the webs for a particular mounting configuration. The length of the offset, and thus the width of the filler elements, is 6.35 mm. The air gap, which has a height of 0.13 meters, is composed of two layers of solid elements. Therefore, the height of each 3-D fluid element is 0.065m. This gives the filler elements an aspect ratio of approximately 0.1, which is still within the threshold of acceptable elements in MSC/NASTRAN, but small enough so that the effect of these additional elements on the dynamics on the panel is insignificant. A close-up of the finite element model is shown in Figure 34. This figure shows the transverse edge of the panel around the center stiffener. The small circles show the RBE2 rigid body constraints which span the width of the filler elements.

3.4: Study of Trim Panel Mounting Configuration

This study examines two possible mounting configurations for attaching the trim panels to the primary structure. The first case is the one shown in Figure 32, in which the corners of the trim panels are pinned to the edges of the webs at the six endpoints of the stiffeners. Thus there would be eight rigid body elements which constrain the translations of the trim panel in the model. The grid point nodes of the webs at the points of attachments were defined to be the independent nodes while the corresponding grid point nodes of the trim panels were defined to be the constrained dependent nodes. The second configuration studied the case in which the trim panel is pinned with a rigid body element at every grid point node along the transverse edges to the corresponding grid point nodes of the webs. This case is shown in Figure 35. Once again the web nodes were the independent nodes and the trim panel nodes were the dependent ones.

For the built-up curved honeycomb panel, it is very difficult to recognize or name the mode shapes due to the complex physical geometry of the model. The addition of the trim panels added many new resonances to the structure. Most of these new resonances are modes of the trim panels alone. In an effort to indicate the frequencies of these trim panel modes, a frequency response analysis was performed in which the normal velocities of three grid points on the trim panels were calculated. One of these points was located in the center of one of the trim panels, and the other two were located near the centers of two different quadrants of the same trim panel. Since there is longitudinal symmetry in the panel, it is only necessary to study the response of one of the trim panels. Three different points were chosen in order to “capture” all the modes of the trim panel in the frequency range The normal velocities for the three grid points were calculated over the

whole frequency range and the "power," which is defined here to be vv* where v is the normal velocity at the grid point, was subsequently calculated. Figure 36 shows the power spectral density for the three chosen grid points for the case in which the trim panel is pinned at the corners. Figure 37 shows the power spectral density for the case in which the trim panel is attached along the transverse edges. The peaks in these curves indicate the frequencies at which trim panel modes occur.

The modal characteristics of the primary structure are not significantly altered by the addition of the trim panel and by the fluid-structure coupling. Figure 38 shows power spectral density curves for a grid point located on the response side face sheet of the primary structure, for the three different configurations. Only one grid point was chosen so that the figure would be not be too cluttered. Note that the grid point chosen was located near the center of one of the quadrants of the bays of the panel. Note that since only one grid point was studied here, all the modes of the primary structure are not indicated in the figure. Figure 38 shows that the panel modes, which are excited at all three grid points, undergo only a very small shift in frequency and that the magnitude of the response of the primary structure does not vary significantly for the different cases.

A transmission loss analysis was performed on the panel for all three configurations. The goal was to use a reverberant field as the excitation. Because of the extensive computation time required to force each node on the incident side of the panel individually as described in Section 2.5, this reverberant field was approximated by sixteen patches of nodal forces on the incident side of the panel. The panel's structural response was calculated at each grid point on the response side face sheet for the bare panel case, and at each grid point on the trim panels for the two trim panel mounting

configurations. The input power for all three cases was assumed to be unity. Thus, the transmission loss values are actually a relative transmission loss. This is sufficient since this study is only concerned with the trim panel's effect on the transmission loss relative to the bare panel case. The results are shown in Figure 39.

Figure 39 shows that the transmission loss is increased by almost 10 dB throughout the damping controlled region of the primary structure for the case in which the trim panel is attached to the primary structure only at the corners. The other mounting configuration for which the edges of the trim panel are pinned along the length of the webs yields similar results, although the transmission loss is a few decibels lower than for the first trim panel case over various frequencies throughout the range.

The finite element model for the built-up curved honeycomb panel was further enhanced by the addition of fluid damping in the air gaps between the primary structure and the trim panels. This is a first approximation to the effect of acoustical damping treatments such as blankets or fiberglass in the gap. This damping factor was included in the MSC/NASTRAN bulk data file by assigning a non-zero value to the parameter GFL. In this case it was assumed that the fluid damping coefficient is .30. Figures 40 and 41 show the power spectral density for the two trim mounting configurations, using the same grid point nodes on the trim panels as for the non-damped cases. The curves for the non-damping cases are included in the figures for comparison. As expected, the addition of fluid damped causes a decrease in the dynamic response of the panel at each of the three grid points. Figure 42 shows the relative transmission loss as a function of frequency for these cases. These curves are shown against the non-damped curves of Figure 39. This figure shows that the addition of fluid damping, which shares some of the same noise

transmission, characteristics as the addition of acoustical blankets, causes an increase in transmission loss of about 3-7 dB for both trim panel mounting configurations in the damping controlled frequency region. Also, several of the modes of the trim panel, which occur near the frequencies indicated by valleys in the transmission loss curves, have been slightly “damped out” by the addition of fluid damping.

4. Conclusions

4.1: Discussion of Results

This paper has considered only a very small part of the passive noise control research which will be conducted in the High Speed Research Program. Despite the need for extensions and continuation of this work, which will be discussed in the next section, there are some very valuable points which can be taken from this study.

This study devoted a large part of its focus to finite element model development and validation. The procedures and assumptions made in the development of the finite element model for the honeycomb sandwich panels and for the built-up trimmed panels, utilized the fluid-structure coupling capabilities of MSC/NASTRAN. Although they are not new in terms of previously performed research, they can serve as an example for the modeling of similar sidewall panel constructions.

It was concluded that the length scale of adjacent patches necessary to adequately simulate random excitation is on the order of the width of one element in a finite element model with a medium mesh density. As a first approximation of random excitation, however, the length scale can be increased to include several element widths.

The transmission loss results indicate that there are noise control benefits to be reaped by adding trim panels to the sidewalls of interest. Though the actual transmission loss gain achieved by adding the trim panels is only up to about 10 dB across the frequency range, this study indicates that there are other parameters and configurations which can be studied and manipulated to achieve greater transmission loss. The results for the model with fluid damping, for example, show that there is much to be gained by studying the effect of adding other acoustical treatment materials to the panels.

4.2: Possible Improvements and Future Work

Much of what has been done in this study can be considered groundwork for a more in-depth investigation of passive noise control treatments for candidate aircraft sidewall panels. There are several extensions of this work which would fit into the goals of this part of the High Speed Research Program.

First and foremost, as stated in the introduction, the main excitation of interest in this research program is turbulent boundary layer excitation. Some references in the literature for information on modeling turbulent boundary layer excitation are given as a starting point for this investigation [13-17].

Another extension of this work would be to realistically and accurately model the acoustic blankets and cap strips which were other add-on treatments used in the experimental transmission loss testing. These materials are best modeled as elastic porous materials. Since MSC/NASTRAN cannot currently model such materials, it will be necessary to wait for a future release of COMET/SAFE which can accurately model the non-isotropic structural materials.

The experimental transmission loss tests which were performed on the bare curved honeycomb panel and the built-up curved honeycomb panel were done over a frequency range which went up to 6 KHz. The current finite element model does not allow a fine enough mesh to accurately represent the response of the panel for such high frequencies. Increasing the mesh density would increase the computation time, but it may be worth looking into since these higher frequencies are of interest in the noise control efforts.

In this paper, a simple study of the trim panel mounting configuration was performed. Aside from the mounting details, there are other parameters of interest such as the material properties of the trim panel, its thickness, as well as the properties of the additional acoustic insulation materials which were not considered here. Ideally, an optimization of certain key parameters would provide the most useful information for the High Speed Research Program.

Bibliography

[1] Hay, J.A. "Problems of Cabin Noise Estimation for Supersonic Transports," Journal of Sound and Vibration. Volume 1, Number 2, April 1964, pp. 113-126.

[2] Crocker, M.J. "The Response of a Supersonic Transport Fuselage to Boundary Layer and to Reverberant Noise," Journal of Sound and Vibration, Volume 9, Number 1, 1969, pp. 6-20.

[3] Grosveld, F.W., Mixson, J.S. "Noise Transmission Through an Acoustically Treated and Honeycomb Stiffened Aircraft Sidewall," AIAA Paper 84-2329, 1984.

[4] Tang, Y.Y., Silcox, R.J., Robinson, J.H. "Sound Transmission Through Cylindrical Shell Structures Excited by Boundary Layer Pressure Fluctuations," 2nd AIAA/CEAS Aeroacoustics Conference, State College, PA, AIAA Paper 96-1760, 1996.

[5] Tang, Y.Y., Robinson, J.H., Silcox, R.J., "Sound Transmission through a Cylindrical Sandwich Shell with Honeycomb Core," The 34th AIAA Aerospace Meeting and Exhibit, Reno, NV, AIAA Paper 96-0877, 1996.

[6] Bolton, J.S., Green, E.R. "Sound Transmission Through Double Panel Constructions Lined with Elastic Porous Materials," AIAA 10th Aeroacoustics Conference, Seattle, Washington, July 1986, AIAA Paper 86-1907.

[7] Bolton, J.S., Shiau, N.M. "Oblique Incidence Sound Transmission through Multi-Panel Structures Lined with Elastic Porous Materials," AIAA 11th Aeroacoustics Conference, Palo Alto, CA, October 1987, AIAA Paper 87-2660.

[8] Bolton, J.S., Shiau, N.M. "Random Incidence Transmission Loss of Lined, Finite Double Panel Systems," AIAA 12th Aeroacoustics Conference, San Antonio, TX, April 1989, AIAA Paper 89-1048.

[9] Attenborough, K. "Acoustical Characteristics of Porous Materials, " Physics Reports, Volume 82, No. 3, 1982, pp. 179-227.

[10]Lahey, R. S., et al., editors. MSC/NASTRAN Reference Manual, Version 68, Volume 1, The MacNeal-Schwendler Corporation, 1994.

[11]Reymond, M., Miller, M., Editors. MSC/NASTRAN Quick Reference Guide, Version 68. The MacNeal-Schwendler Corporation, 1994.

[12]Leissa, A.W. Vibration of Plates, NASA SP-160, 1969.

[13]Graham, W.R. "Boundary Layer Induced Noise in Aircraft, Part I: The Flat Plate Model," Journal of Sound and Vibration, Volume 192, Number 1, 1996, pp. 101-120.

[14]Graham, W.R. "Boundary Layer Induced Noise in Aircraft, Part II: The Trimmed Flat Plate Model," Journal of Sound and Vibration, Volume 192, Number 1, 1996, pp. 121-138.

[15]Efintsov, B.M. "Characteristics of the Field of Turbulent Wall Pressure Fluctuations at Large Reynolds Numbers," Soviet Phys. Acoust., Volume 28, Number 4, July-August 1982, pp. 289-292.

[16]Corcos, G.M. "The Structure of Turbulent Pressure Field in Boundary-Layer Flows," Fluid Mechanics, Volume 18, 1964, pp. 353-378.

[17]Graham, W.R. "A Comparison of Models for the Wavenumber-Frequency Spectrum of Turbulent Boundary Layer Pressures, " Journal of Sound and Vibration, Volume 206, Number 4, 1997, pp. 541-565/

[18]COMET/Acoustics User Document, Automated Analysis Corporation, Ann Arbor, MI, 1998.

[19]Fahy, F. Sound and Structural Vibration. Academic Press, London, 1985.

[20]Crowley, J.R., Hunt, D.L., Rocklin, G.T., Vold, H. "The Practical Use of the Polyreference Modal Parameter Estimation Method," 3rd International Modal Analysis Conference, Schenectady, NY, January 1985.

[21] Fernholz C.M., Robinson, J.H. "Fully-Coupled Fluid/Structure Vibration Analysis Using MSC/NASTRAN," NASA Technical Memorandum 110215, January 1996.

Appendix A

In a frequency response analysis, the equation of motion for the structure can be written [10]

$$[M_s]\{\ddot{u}\} + [B_s]\{\dot{u}\} + [K_s]\{u\} = e^{i\omega t}[F(\omega)] \qquad \textbf{(A1)}$$

in which F(ω) is a harmonic excitation of the structure and $[B_s]$ is the structural damping matrix. Assuming a steady-state harmonic solution, Equation [A1] becomes

$$(-\omega^2[M_s] + i\omega[B_s] + [K_s])\{u(\omega)\} = [F(\omega)] \qquad \textbf{(A2)}$$

Note that in these equations, ω represents the excitation frequency of the system.

Three-dimensional elements are used to model fluids in a finite element analysis. The nodes of these elements each have one degree of freedom. The equation of motion of the fluid in a frequency response analysis is [12]

$$[M_f]\{\ddot{p}\} + [K_f]\{p\} + \rho_f[C]\{\ddot{u}\} = [0] \qquad \textbf{(A3)}$$

where $[M_f]$ is the acoustic "mass" matrix and $[K_f]$ is the acoustic "stiffness" matrix. The motion of the structure is coupled to the acoustic pressure in the fluid by the [C] matrix. The boundary condition at the fluid structure interface is

$$\frac{\partial p}{\partial n} = -\rho_f \frac{\partial^2 u_n}{\partial t^2} \qquad \textbf{(A4)}$$

in which n is the unit vector oriented normal to the surface of the structure. Also, ρ_f is the fluid density and u_n is the displacement of the structure in the normal direction. This boundary condition is considered in the third term of Equation [A3]. The fluid affects the structure motion by applying forces

$$\{F_p\} = -[C^T]\{p\} \qquad \textbf{(A5)}$$

over the surface area of the structure.

Thus, the coupled equations of motion of the fluid and structure are

$$\begin{bmatrix} M_s & 0 \\ \rho_f C & M_f \end{bmatrix}\begin{Bmatrix} \ddot{u} \\ \ddot{p} \end{Bmatrix}+\begin{bmatrix} B_s & 0 \\ 0 & 0 \end{bmatrix}\begin{Bmatrix} \dot{u} \\ \dot{p} \end{Bmatrix}+\begin{bmatrix} K_s & -C^T \\ 0 & K_f \end{bmatrix}=e^{i\omega t}\begin{Bmatrix} F(\omega) \\ 0 \end{Bmatrix} \quad \textbf{(A6)}$$

For the frequency response analyses used in this study, the modal method of solution was employed. In this method, it is assumed that the physical variables in the problem, (*p*,*u*), can be written as a linear combination of the uncoupled acoustic and structural modes

$$\begin{aligned} [u] &\approx [\Phi_s][\xi_s(\omega)]e^{i\omega t} \\ [p] &\approx [\Phi_f][\xi_f(\omega)]e^{i\omega t} \end{aligned} \quad \textbf{(A7)}$$

where Φ_s are the uncoupled eigenvectors of the structure, Φ_f are the uncoupled eigenvectors of the fluid, ξ_s are the modal amplitudes for the structure, and ξ_f are the modal amplitudes of the fluid. It should be noted that Equations [A7] are equalities if all of the modes of the system are used. Although, in typical cases, this is not done, and the system is approximated by the first few modes. If these equations are substituted into Equation [A6], and pre-multiplied by the transposed transformation matrix, the result is

$$\begin{bmatrix} \Phi_s^T M_s \Phi_s & 0 \\ \rho_f \Phi_f^T A \Phi_s & \Phi_f^T M_f \Phi_f \end{bmatrix}\begin{Bmatrix} \ddot{\xi}_s \\ \ddot{\xi}_f \end{Bmatrix}+\begin{bmatrix} \Phi_s^T B_s \Phi_s & 0 \\ 0 & 0 \end{bmatrix}\begin{Bmatrix} \dot{\xi}_s \\ \dot{\xi}_f \end{Bmatrix}+\begin{bmatrix} \Phi_s^T K_s \Phi_s & -\Phi_s^T A^T \Phi_f \\ 0 & \Phi_f^T K_f \Phi_f \end{bmatrix}=\begin{Bmatrix} \Phi_s^T F(\omega) \\ 0 \end{Bmatrix}$$

(A8)

APPENDIX B – FIGURES

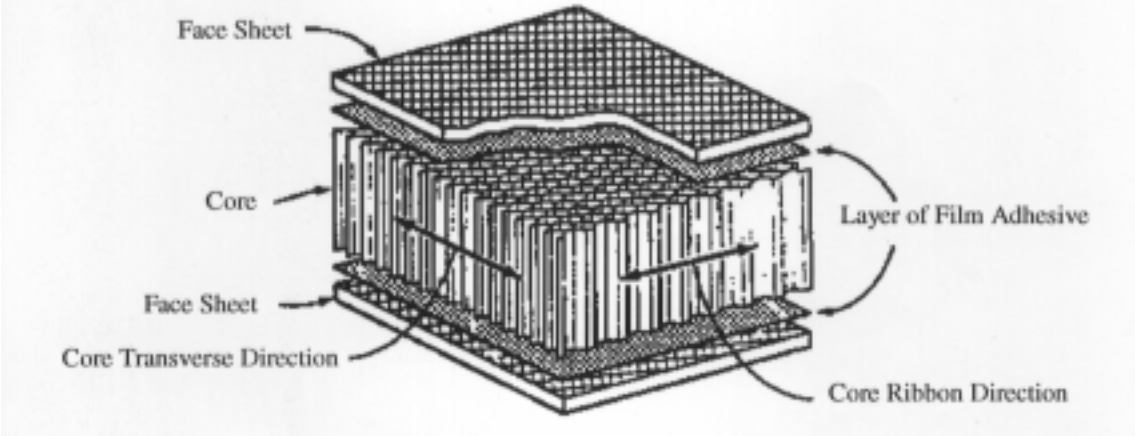

Figure 1 Honeycomb Sandwich Structure

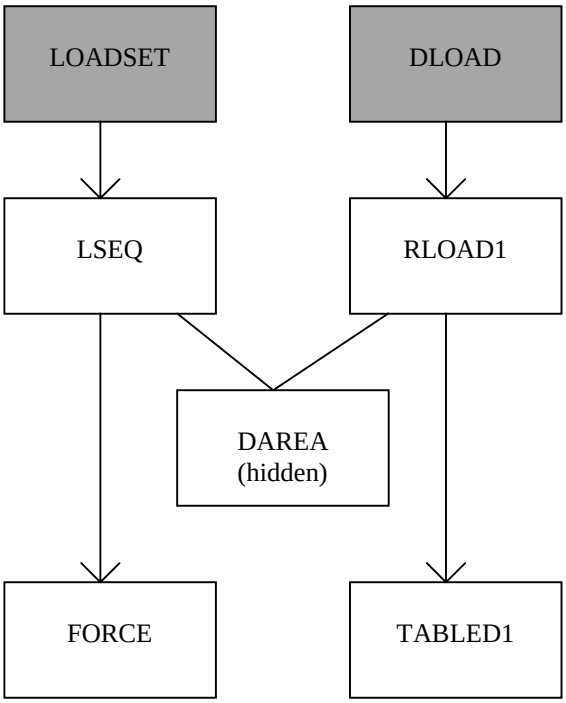

Figure 2 Hierarchy of MSC/NASTRAN bulk data cards used to apply nodal forces to a finite element model. The shaded boxes represent cards which are part of the Case Control. An arrow points from one card to another card, which it references. The MSC/NASTRAN Quick Reeference Guide gives more detail about each of these cards and their usage.

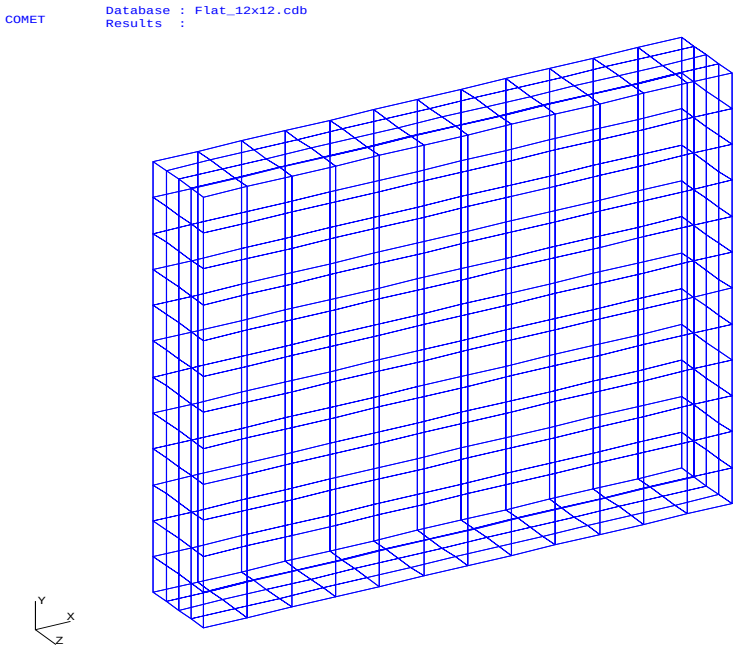

Figure 3 Boundary Element Mesh used to perform the acoustic analysis in COMET/Acoustics for the flat panel geometry. The front surface of the mesh in this figure is the elastic wall, upon which the velocities of the response side of the panel, as determined in MSC/NASTRAN, are imposed.

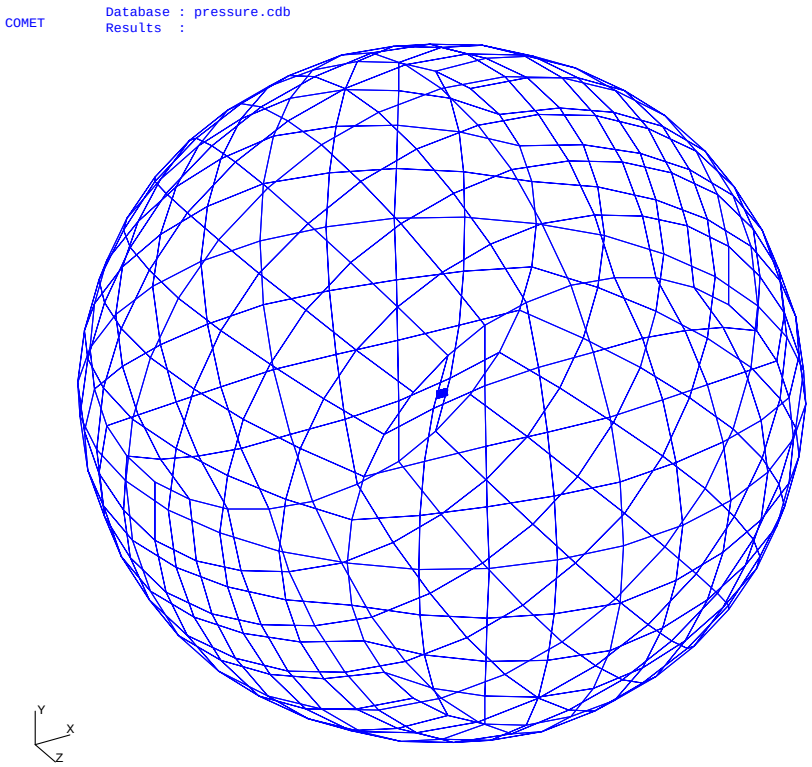

Figure 4 Spherical Data Recovery Mesh used to calculate the acoustic field radiated by the panel. The boundary element mesh is located at the center of the sphere which is 87.0 meters in radius.

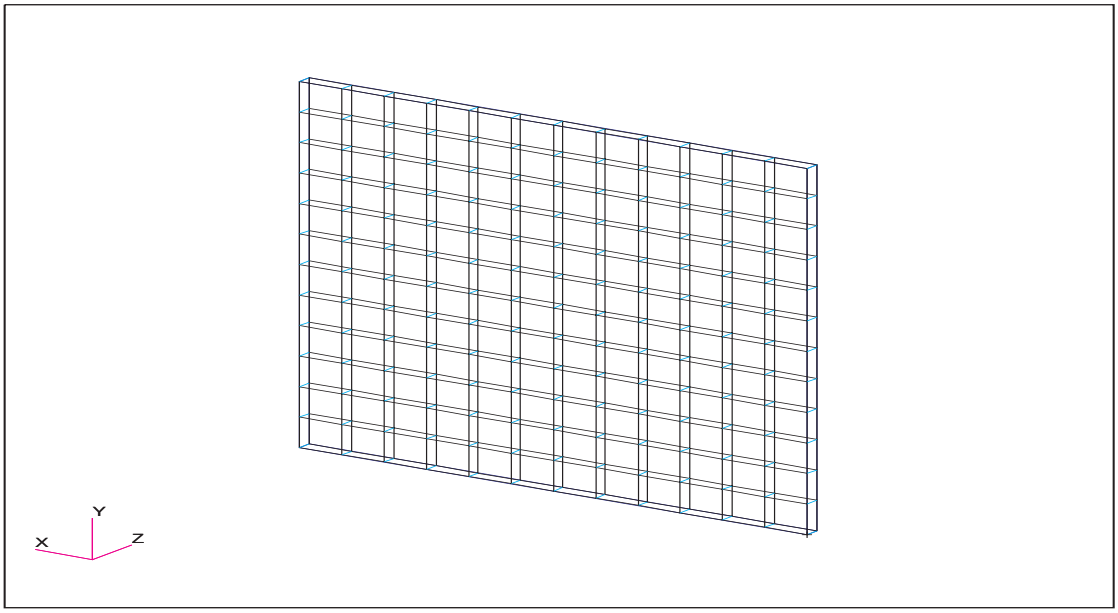

Figure 5 Finite Element Model of Flat Sandwich panel (12x12 Mesh Density). This figure applies to both the isotropic core panel and the honeycomb core panel.

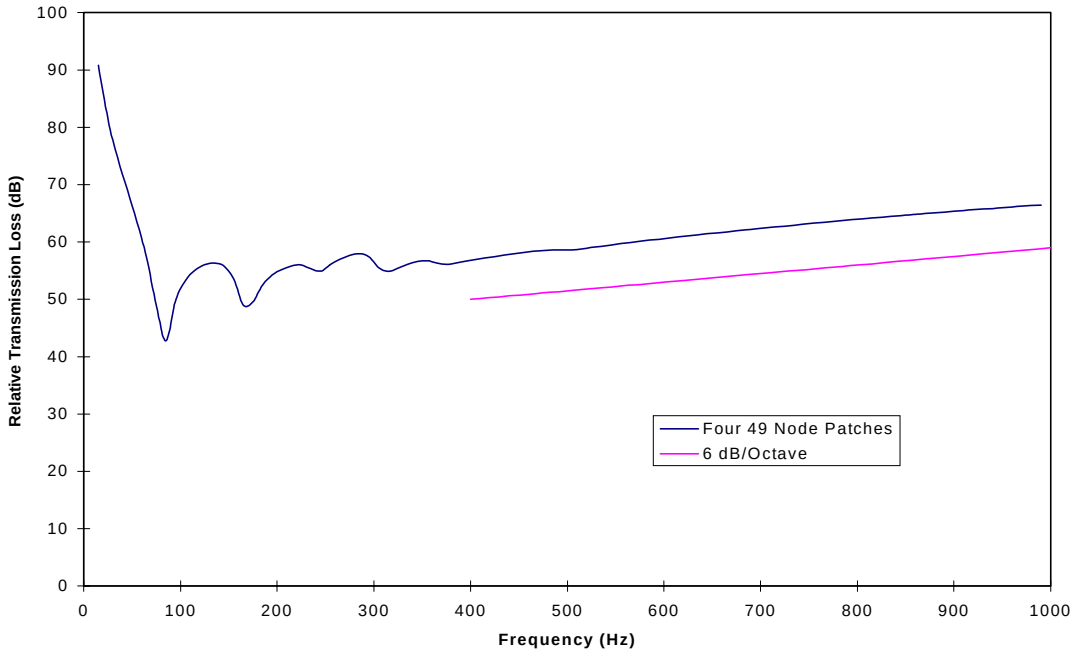

Figure 6 Relative Transmission Loss vs. Frequency for Flat Sandwich Panel with Isotropic Core. This figure demonstrates Mass law behavior in the mass-controlled frequency region.

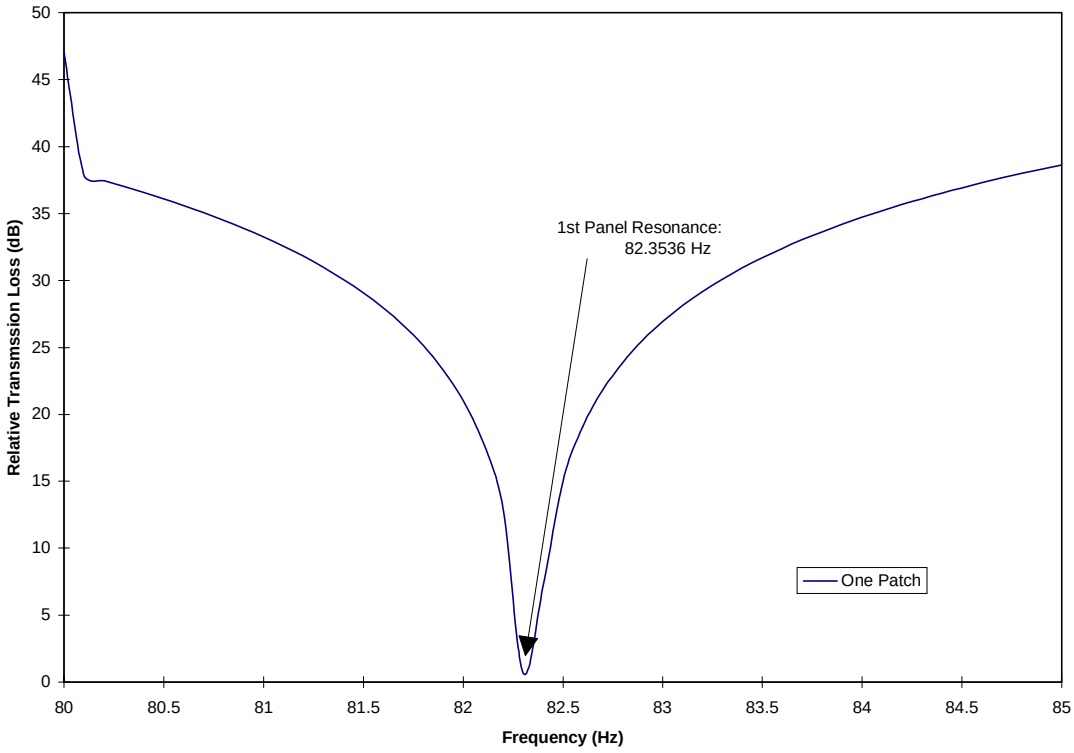

Figure 7 Relative Transmission Loss vs. Frequency for Flat Sandwich Panel with Isotropic Core for frequencies near the first panel resonance – No Damping. Note that the relative transmission loss does not go to exactly zero because the resolution of the frequency range studied was not fine enough to perform the analysis at exactly the resonance frequency.

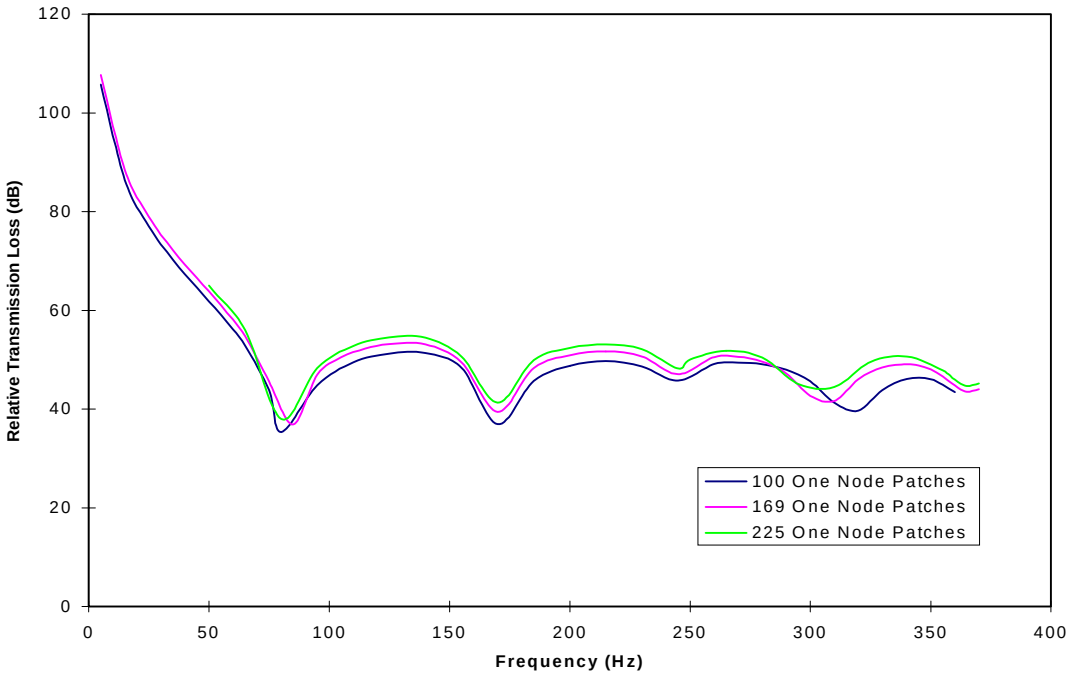

Figure 8 Relative Transmission Loss vs. Frequency for Flat Sandwich Panel with Isotropic Core (5% Damping). This plot shows the curve for three different mesh densities: 9x9 (100 Nodes), 12x12 (169 Nodes), and 14x14 (225 Nodes). This analysis was run for individual nodal uncorrelated forcing.

Figure 9 HSR Flat Honeycomb Panel #261X1423-20

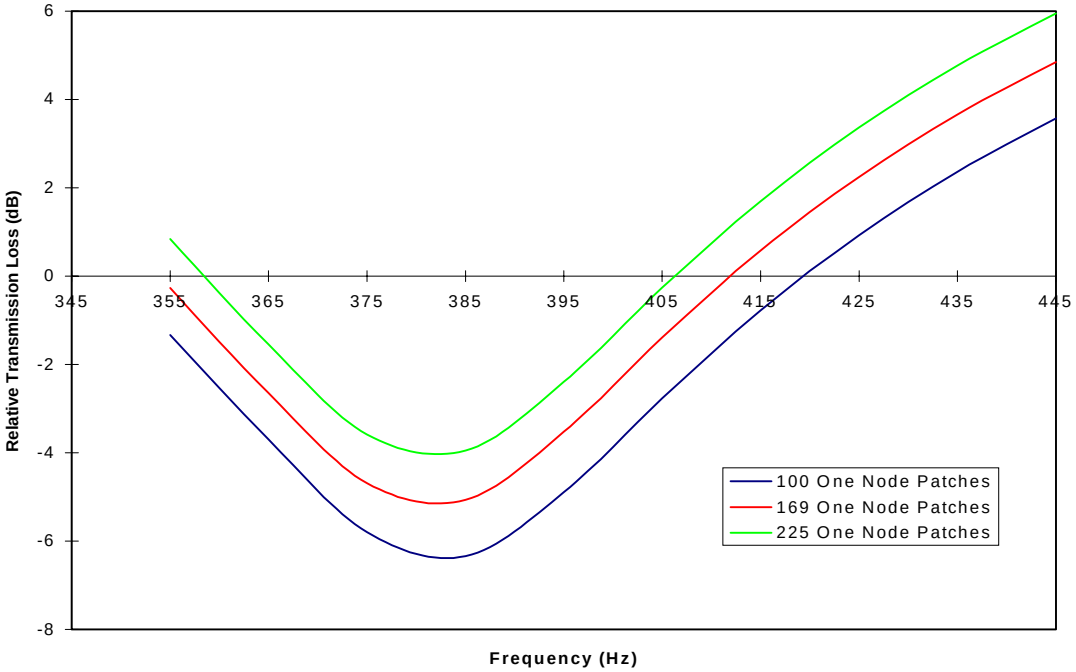

Figure 10 Relative Transmission Loss vs. Frequency for Flat Sandwich Panel with Honeycomb Core (5% Damping). This plot shows the curve for three different mesh densities: 9x9 (100 Nodes), 12x12 (169 Nodes), and 14x14 (225 Nodes). This analysis was run for individual nodal uncorrelated forcing.

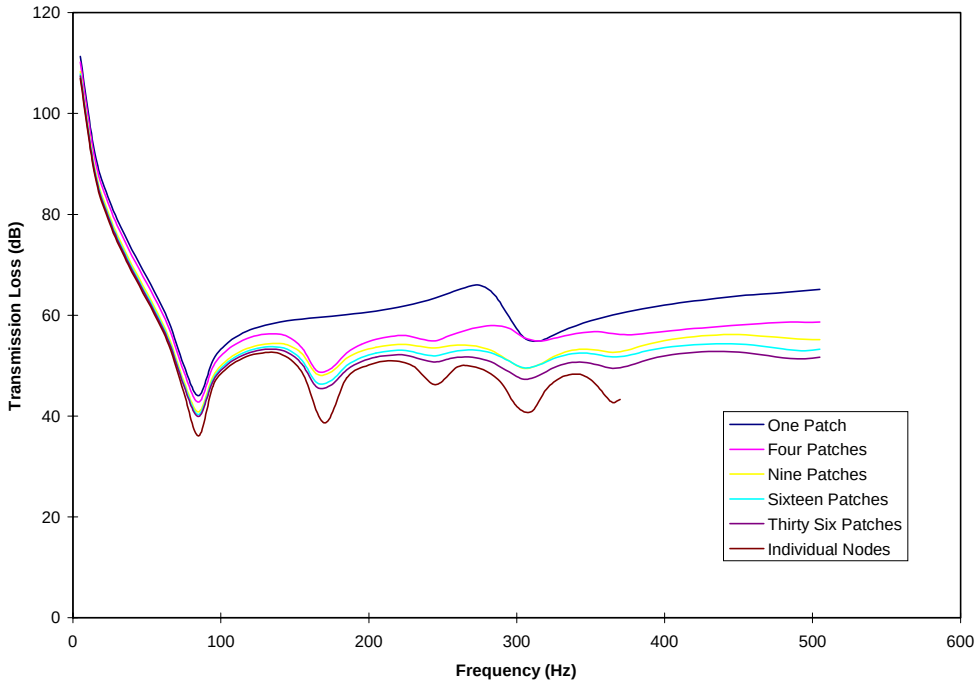

Figure 11 Relative Transmission Loss vs. Frequency for Flat Sandwich Panel with Isotropic Core (5% Damping). The analysis was performed for the following numbers of patches: 1, 4, 9, 16, 36, and 169, where each patch contained 169, 49, 25, 16, 9, and 1 nodes respectively. The force applied per node was 1 N. The mesh density of the incident side of the panel was 12x12 elements.

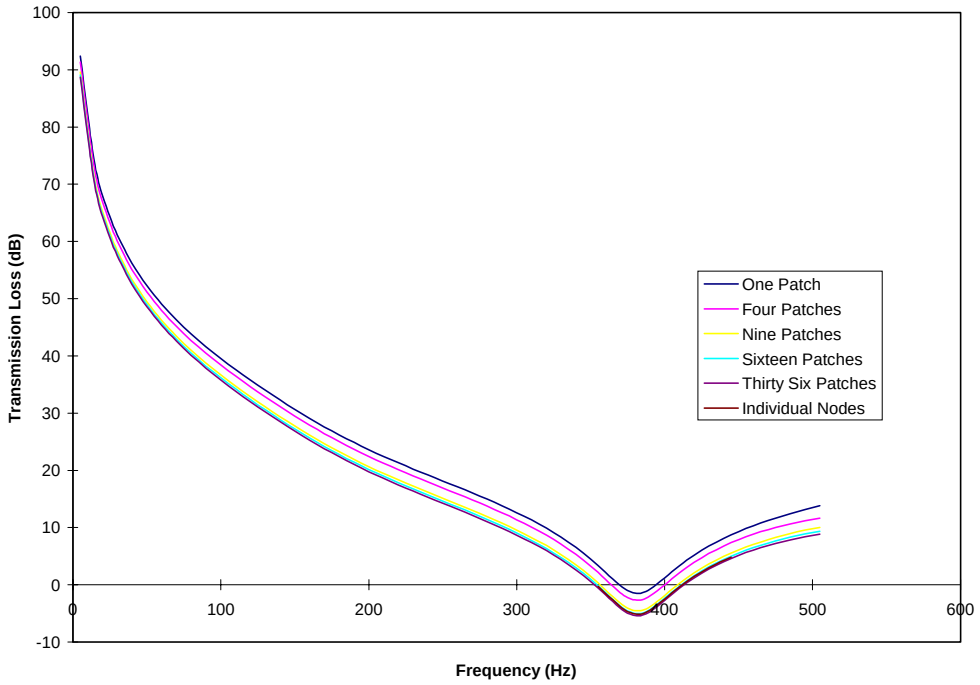

Figure 12 Relative Transmission Loss vs. Frequency for Flat Sandwich Panel with Honeycomb Core (5% Damping). The analysis was performed for the following numbers of patches: 1, 4, 9, 16, 36, and 169, where each patch contained 169, 49, 25, 16, 9, and 1 nodes respectively. The force applied per node was 1 N. The mesh density of the incident side of the panel was 12x12 elements.

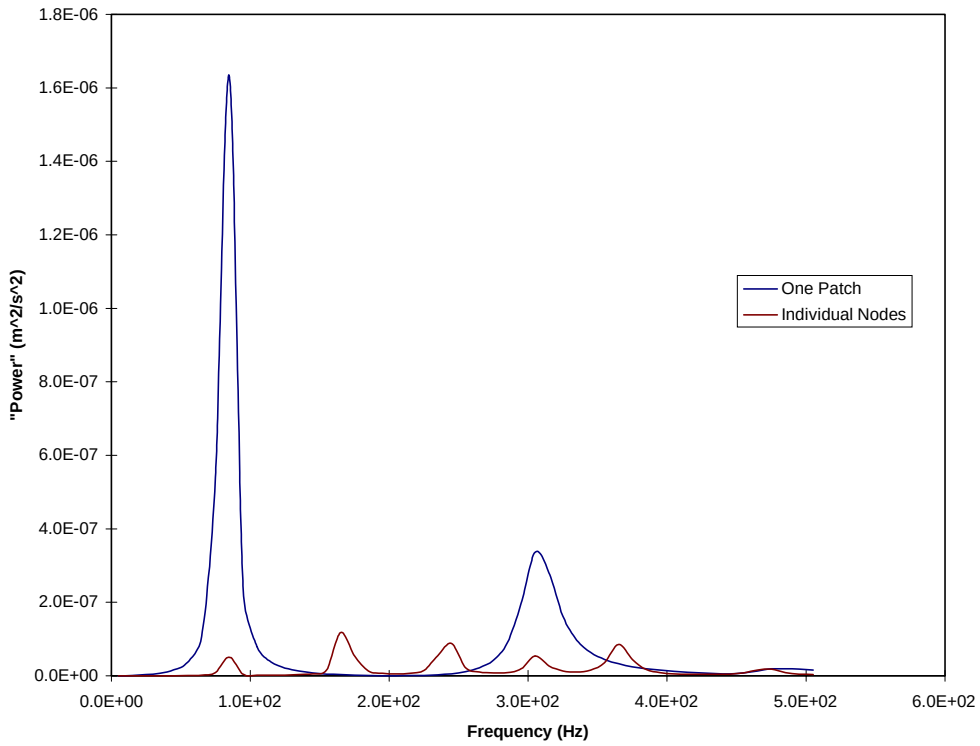

Figure 13 "Power" vs. Frequency for a node on the response side of the flat isotropic core sandwich panel for one patch and individual nodal forcing. The model had 5% structural damping.

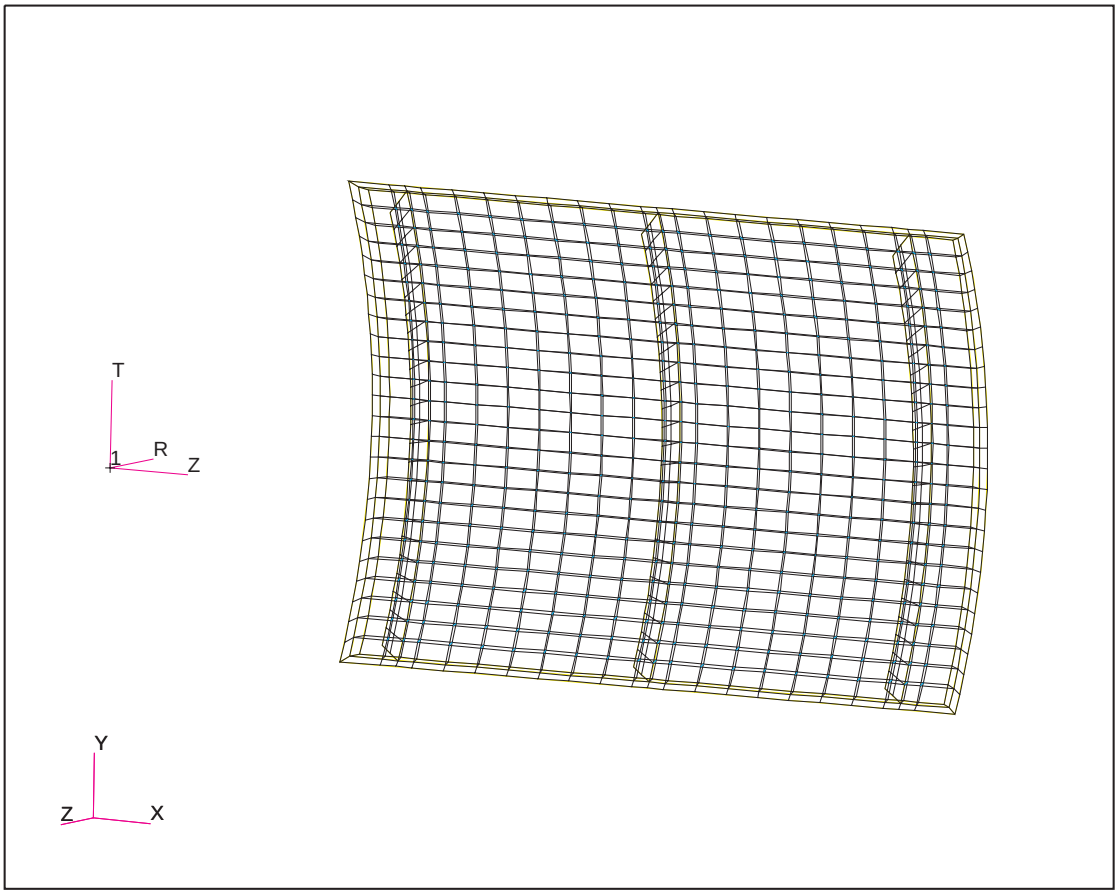

Figure 14 Finite element model for the stiffened, curved honeycomb panel.

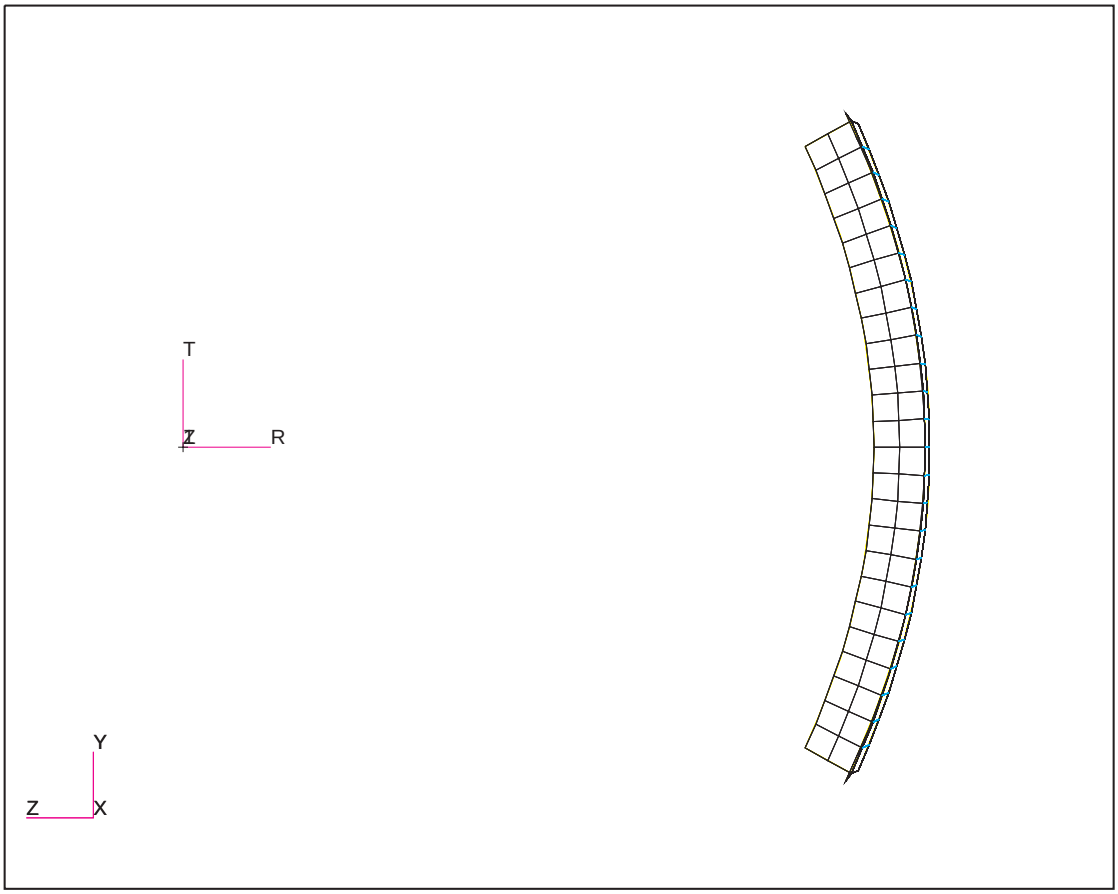

Figure 15 Side view of finite element model for the stiffened, curved honeycomb panel.

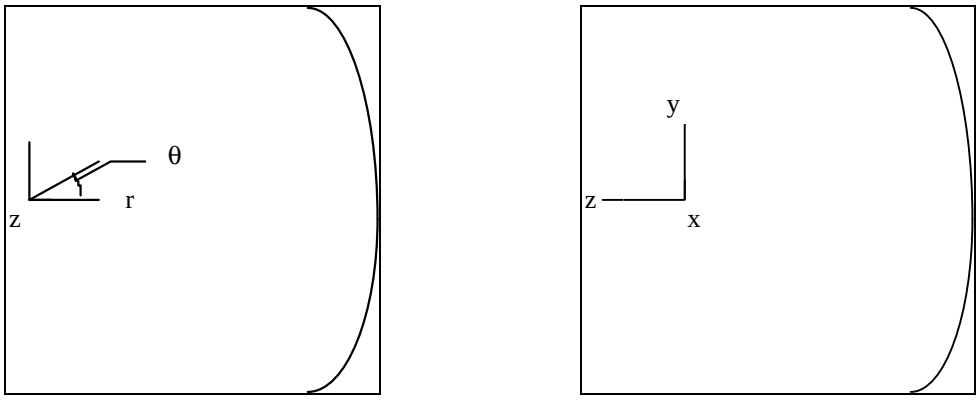

Figure 16 Coordinate systems used in the development of the curved panel finite element model. The first is a cylindrical coordinate system in which the origin is located at the center of the curvatuve of the panel at the longitudinal edge farthest "into the page." The z axis is directed "out of the page." The second figure shows the cartesian coordinate system, which is also has the same origin. The x axis in this system is oriented out of the page.

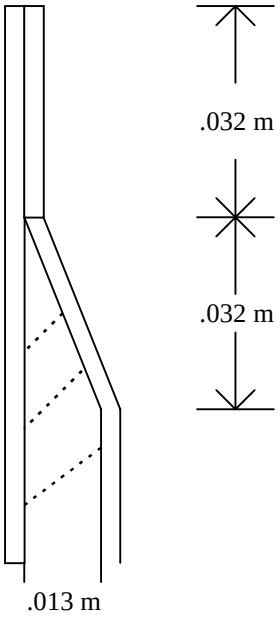

Figure 17 Cross-sectional view of curved panel near edge.

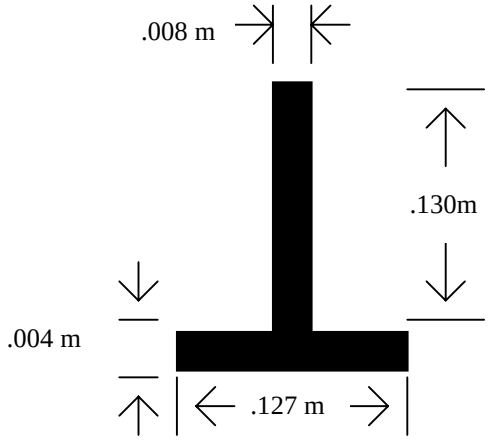

Figure 18 Cross-Sectional view of stiffener. The flange is the horizontal part and the web is the vertical part.

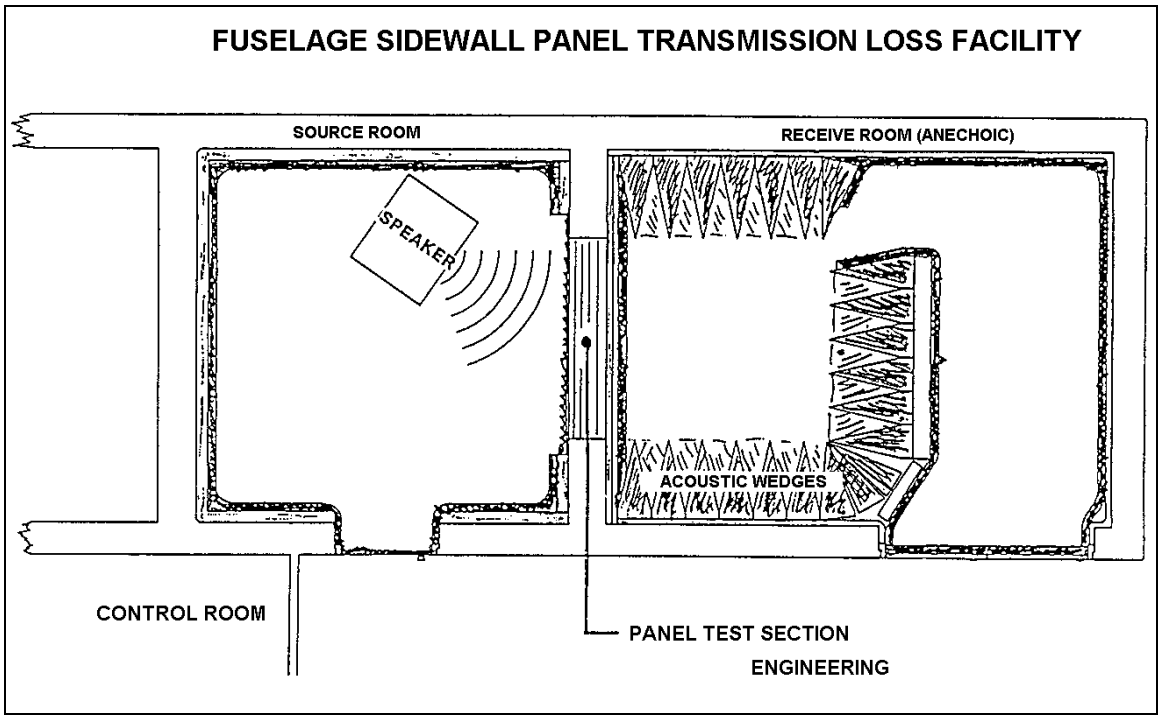

Figure 19 Diagram of the Boeing Company's Transmission Loss Facility.

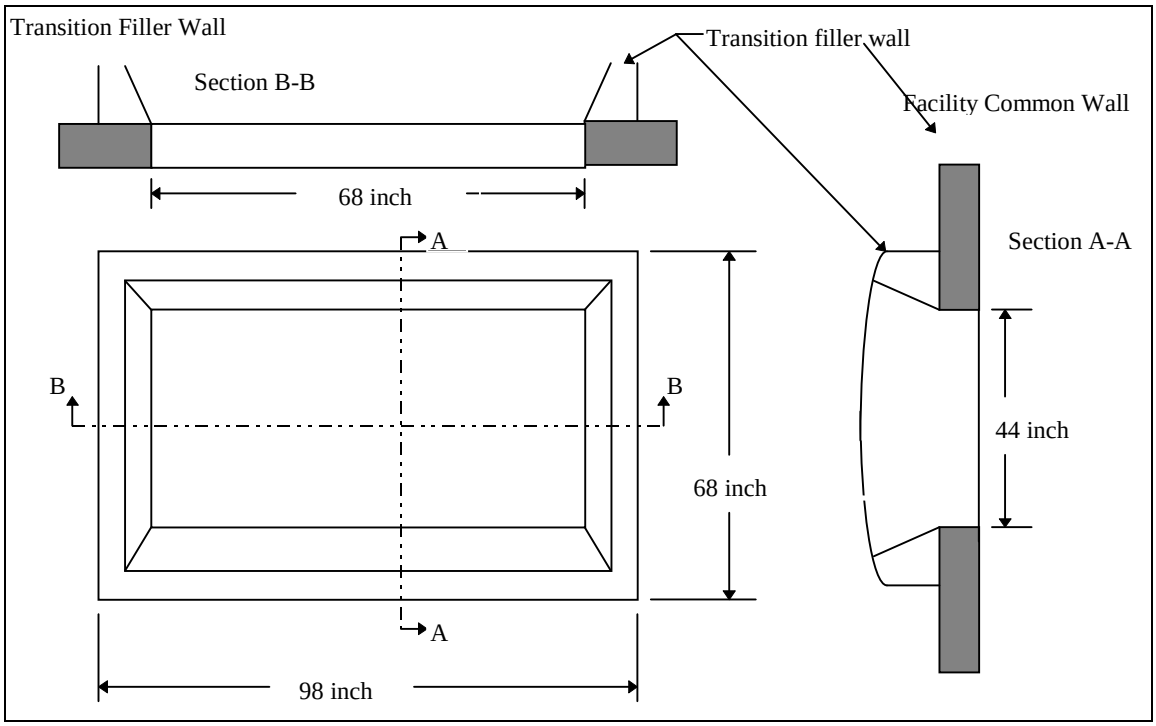

Figure 20 Transition fixture from flat facility wall to test curved honeycomb panel.

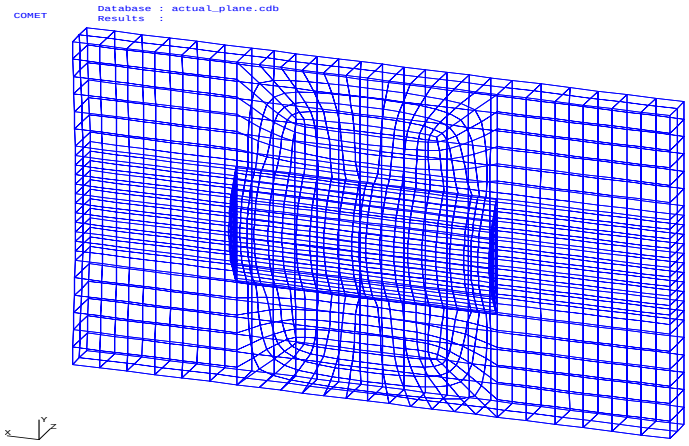

Figure 21 Boundary element mesh used to compute the incident pressures on the curved panel. The center of the source is located at (x,y,z)=(-2.3, 0,-7.8) with direction (dx,dy,dz)=(.5,0,.866).

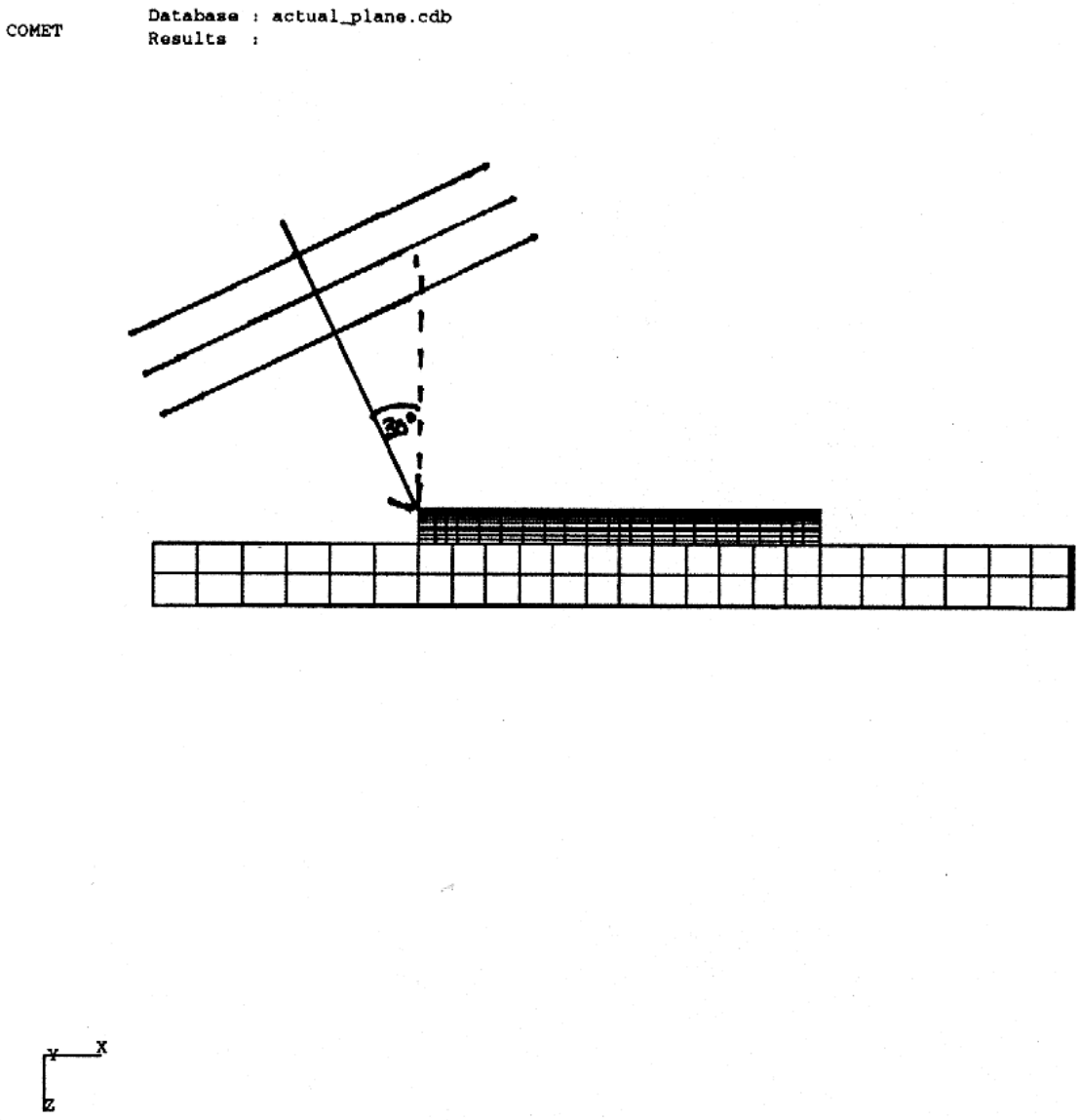

Figure 22 Top view of boundary element mesh used to compute the incident pressures on the curved panel. The plane wave source, which is directed 30 degrees relative to normal incidence on the panel, is shown. Note that the location of the center of the cource is not shown to scale with the rest of the figure.

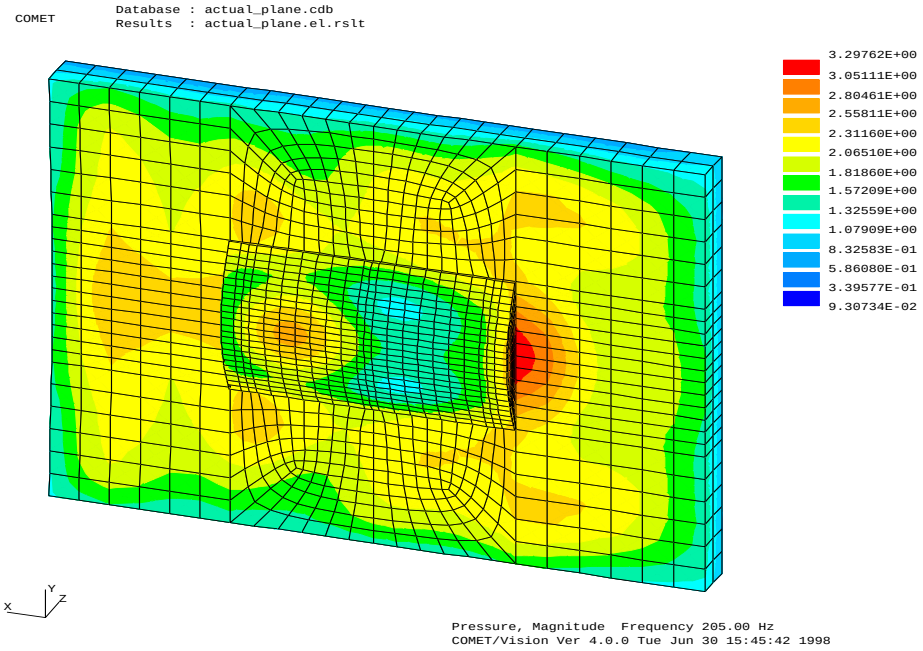

Figure 23 Contour plot of the acoustic pressure magnitude on the boundary element mesh due to an oblique plane wave source at 205 Hz.

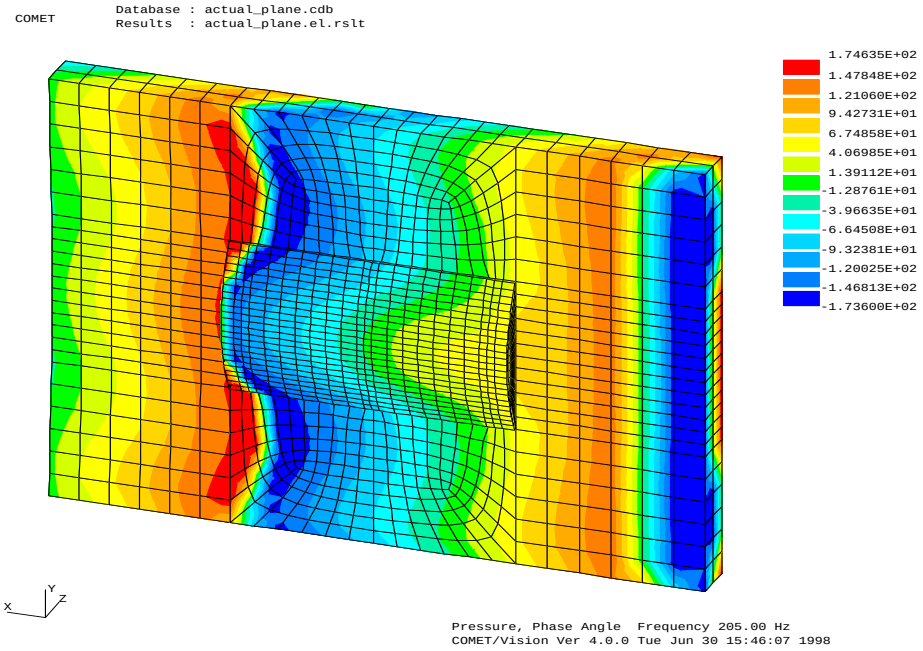

Figure 24 Contour plot of acoustic pressure phase on the boundary element mesh due an oblqiue plane wave source at 205 Hz.

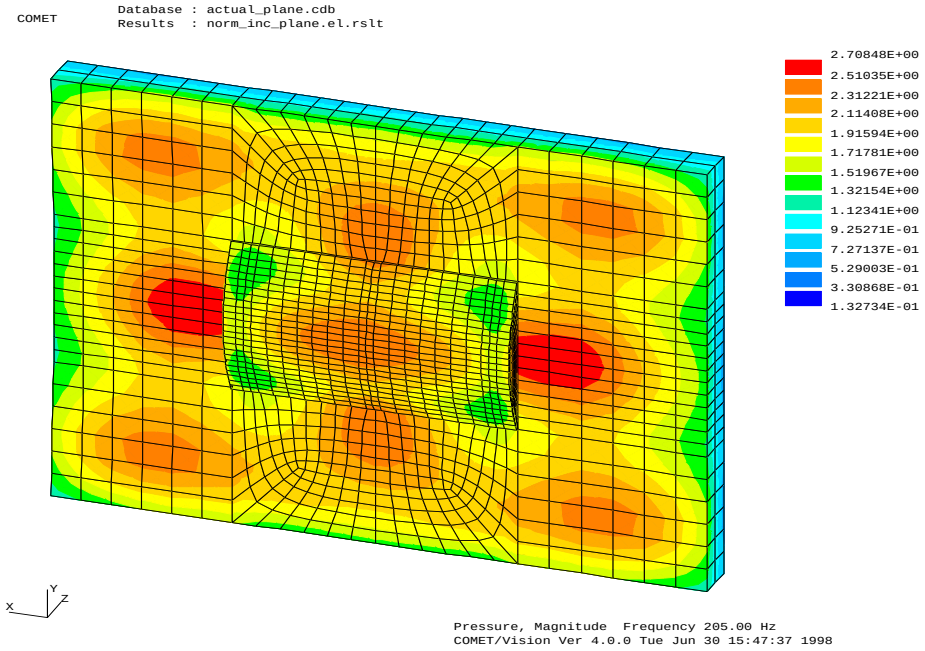

Figure 25 Contour Plot of acoustic pressure magnitude on the boundary element mesh due to a plane wave directed normal to the transverse centerline of the panel and the baffle at 205 Hz.

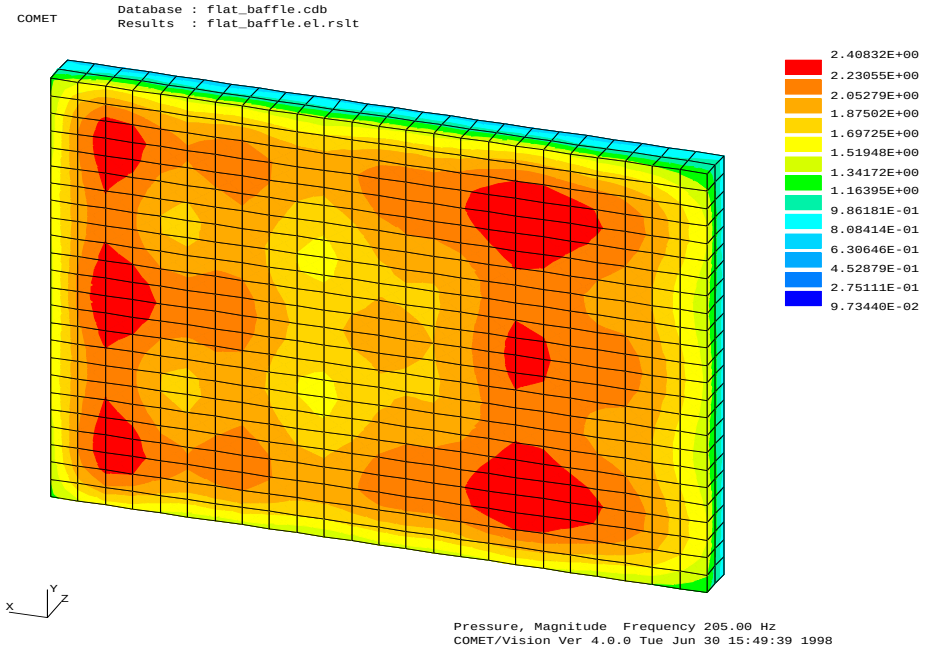

Figure 26 Contour plot of the acoustic pressure magnitude of a flat baffle due to a normal incidence plane wave at 205 Hz.

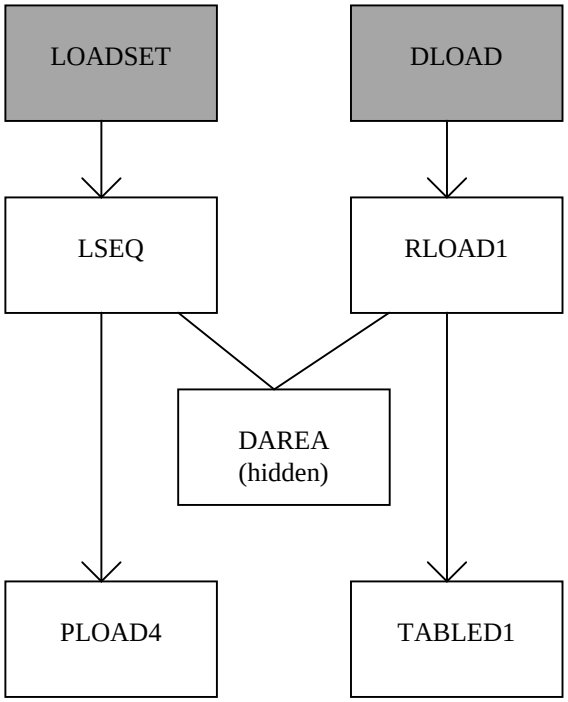

Figure 27 Hierarchy of MSC/NASTRAN bulk data cards to apply elemental pressure on a finite element model. The shaded boxes are the Case Control Commands. An arrow indicates that a certain card references the card to which the arrow points. For more detail about these cards and their usage, consult the MSC/NASTRAN Quick Reference Guide.

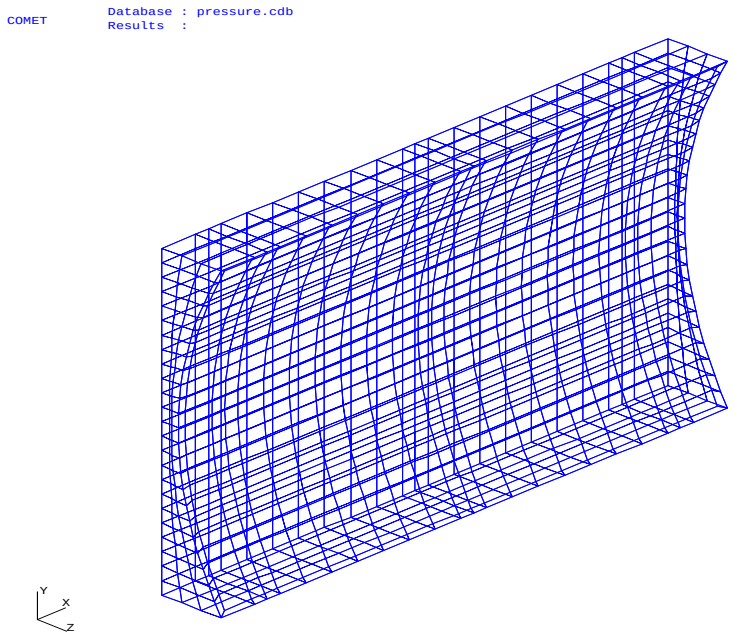

Figure 28 Boundary Element Mesh used to perform the acoustic analysis in COMET/Acoustics for the curved panel geometry. The front surface of the mesh, which is curved, in this figure is the elastic wall, upon which the velocities of the response side of the panel, as determined in MSC/NASTRAN, are imposed.

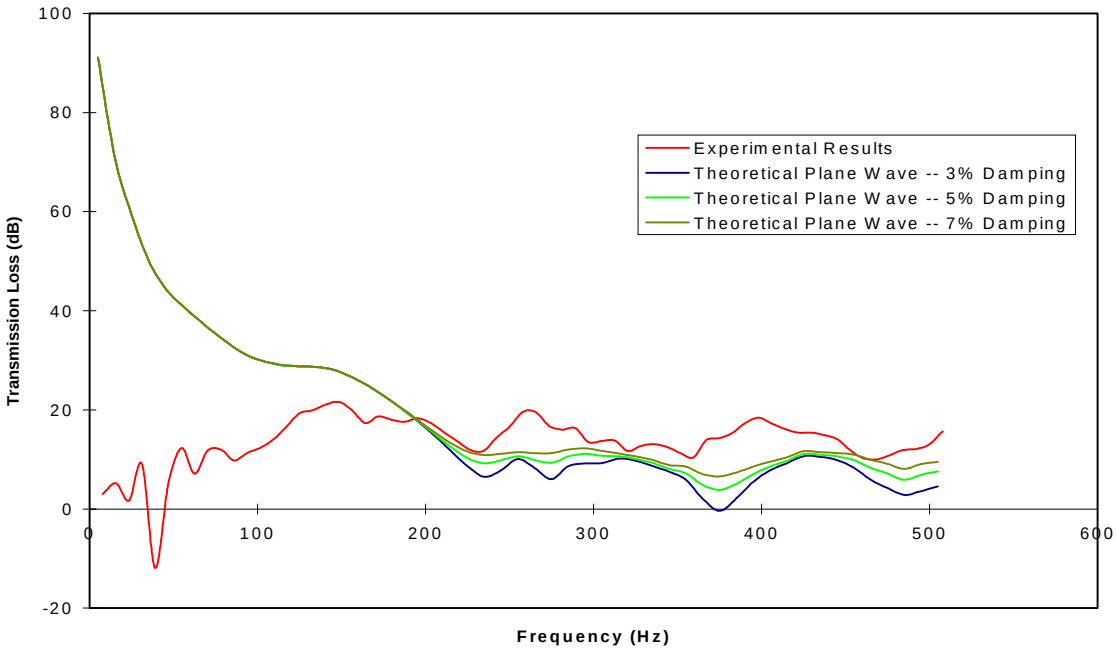

Figure 29 Transmission Loss vs. Frequency for the curved honeycomb panel subjected to oblique plane wave excitation. The edges of the panel are clamped. The model was analyzed for 3%, 5%, and 7% structural damping.

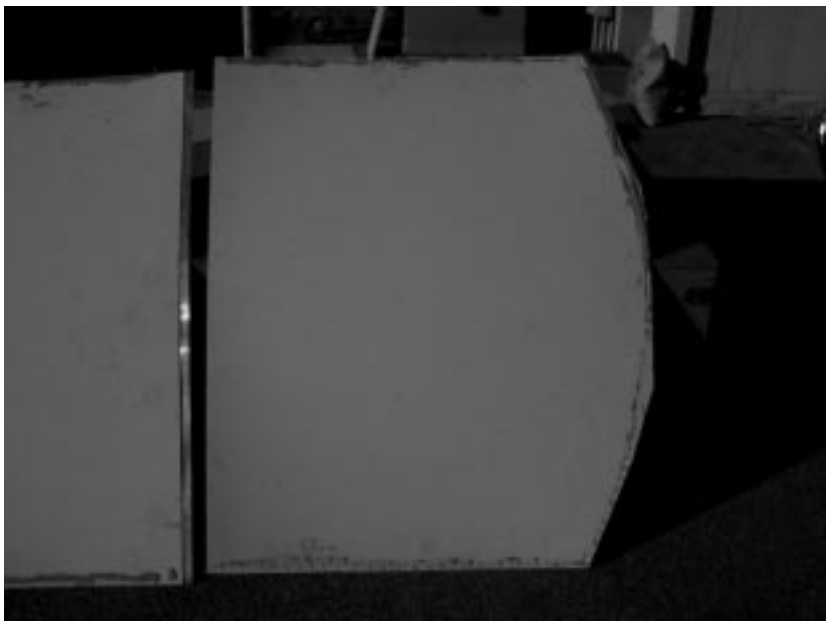

Figure 30 Photograph of trim panels before mounting

Figure 31 Photograph of built-up panel in mounted state.

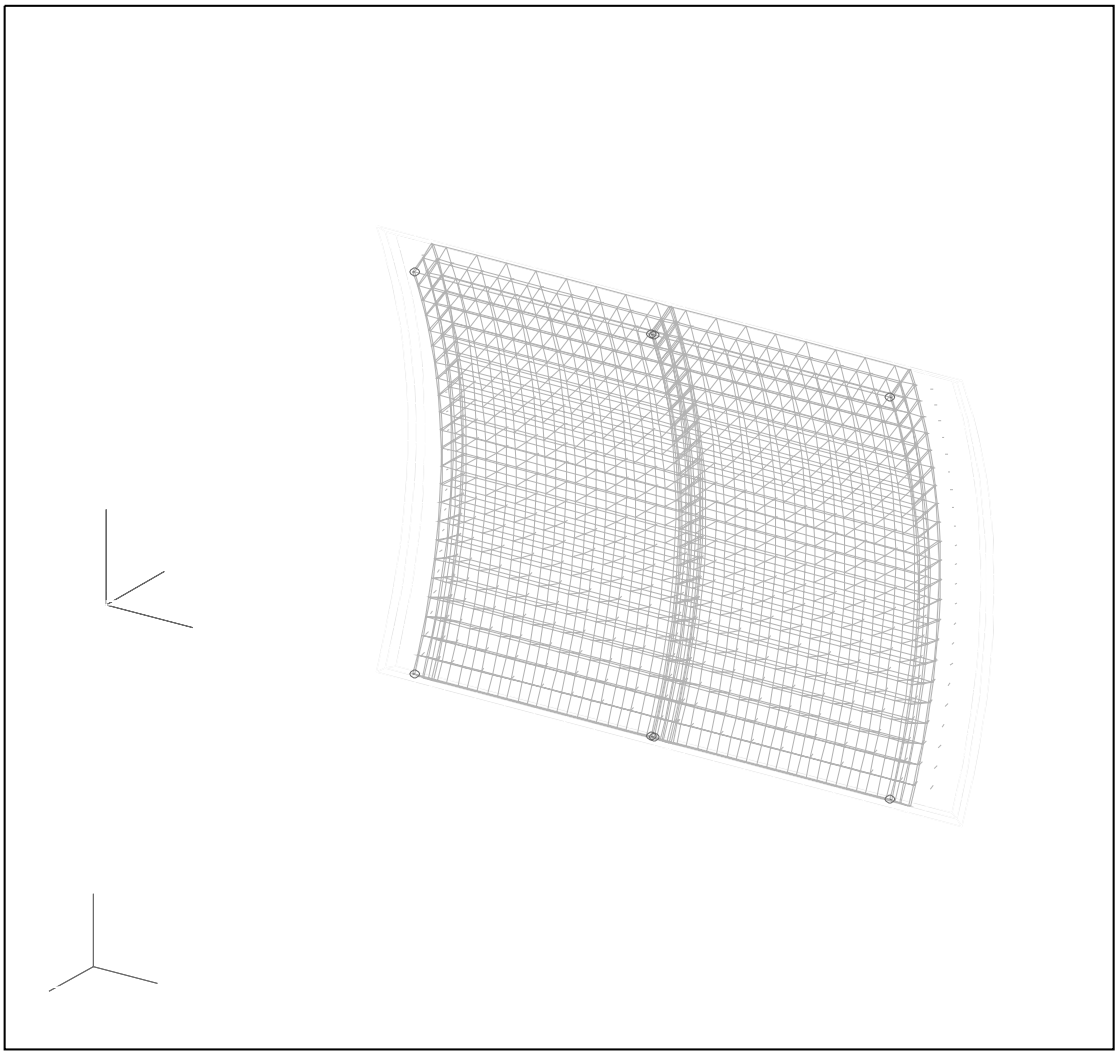

Figure 32 Finite element model for the curved honeycomb panel with trim. In this case, the trim panels are pinned to the webs of the stiffeners of the primary structure only at the corners. The small circles indicate rigid body attachments.

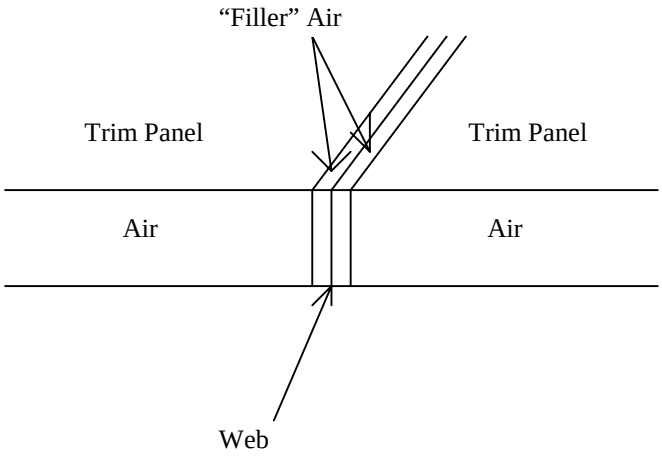

Figure 33 Built-up curved honeycomb panel, showing the "filler" air region which is necessary to properly define the fluid-structure interface in MSC/NASTRAN.

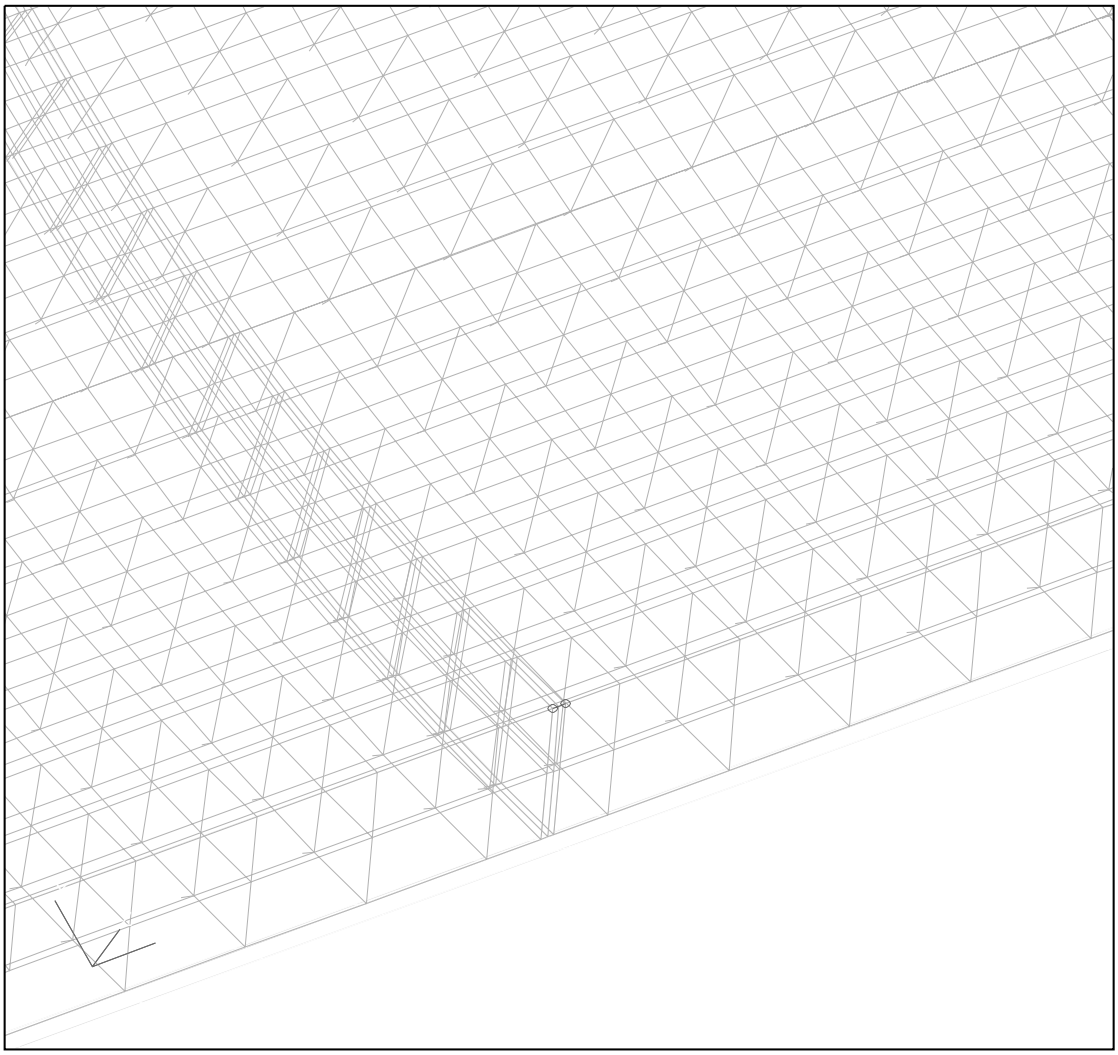

Figure 34 Close-up of the finite element model for the curved honeycomb panel with trim.

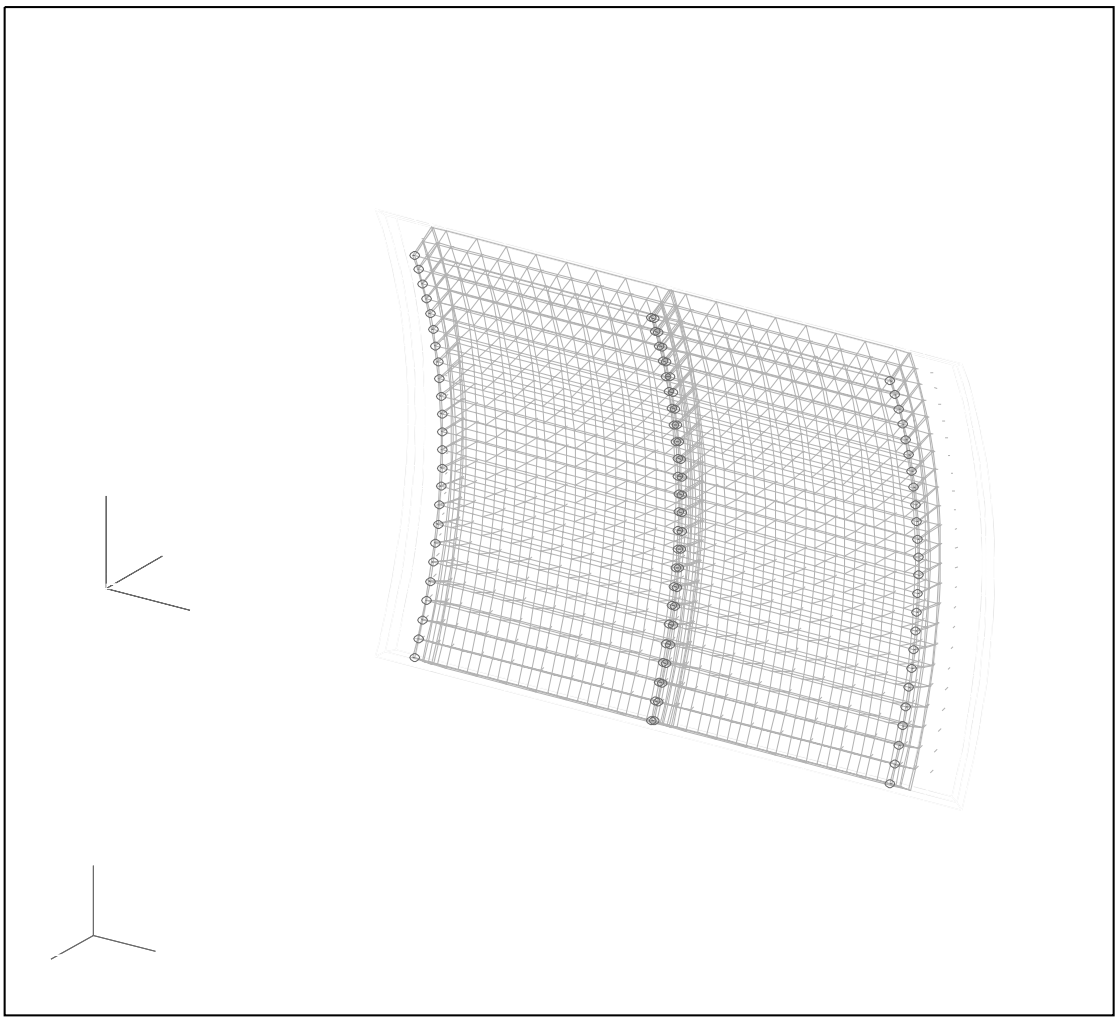

Figure 35 Finite element model of the built-up curved honeycomb panel for the case in which the trim panels are pinned to the webs at every grid point node along their transverse edges. The small circles indicate rigid body attachments.

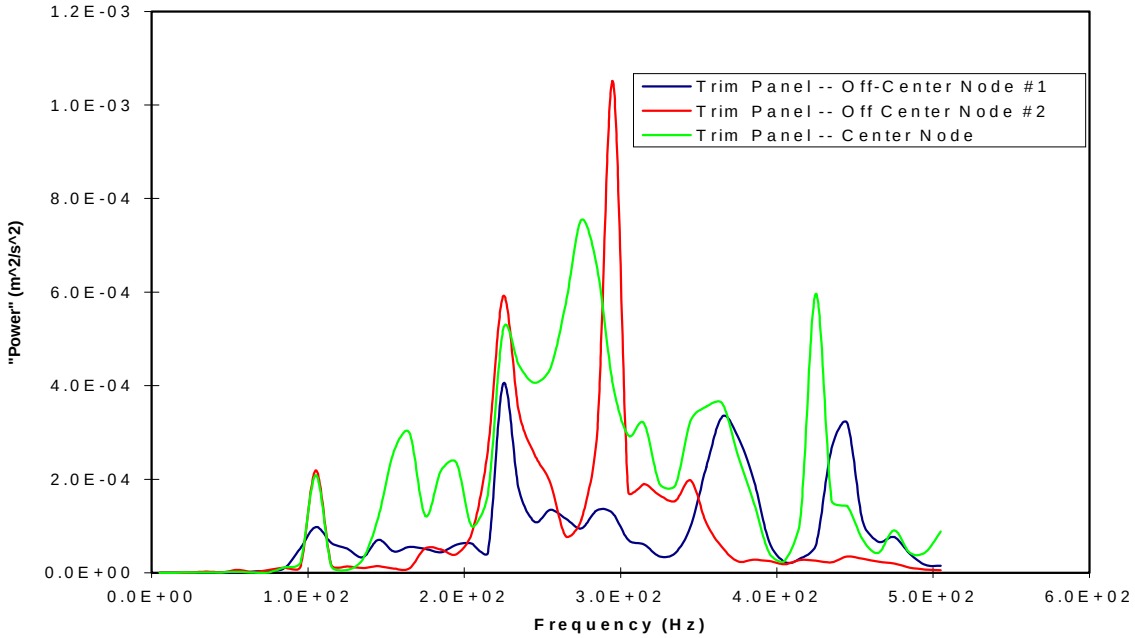

Figure 36 "Power" vs. Frequency for trimmed curved honeycomb panel with trim pinned to primary structure only at the trim panel corners. There is 5% structural damping in the model.

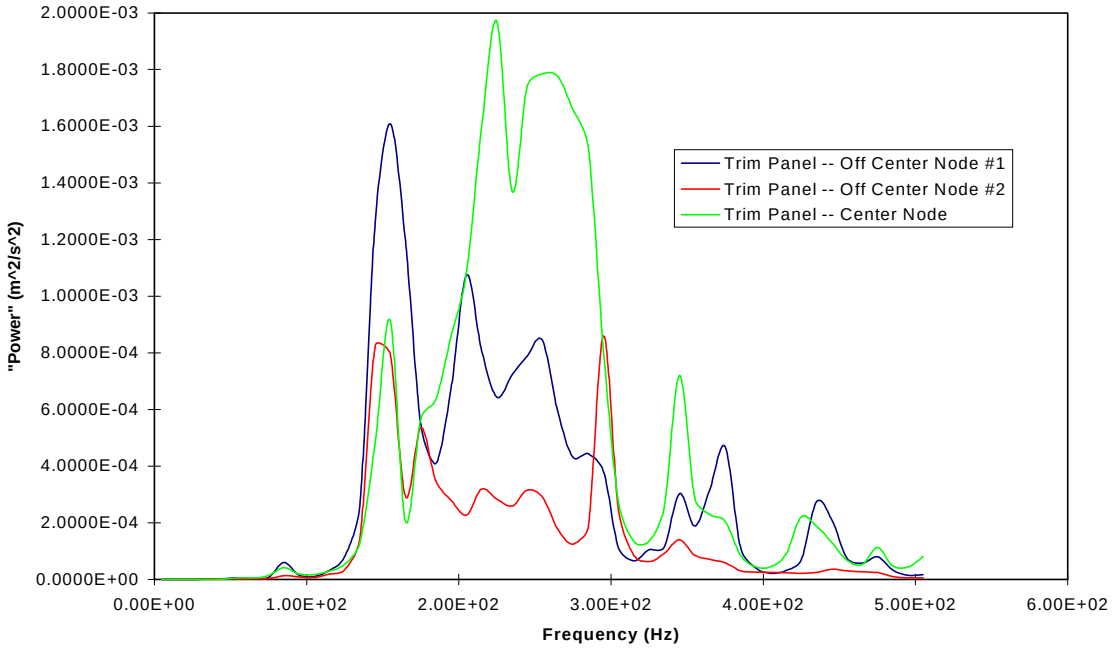

Figure 37 "Power" vs. Frequency for trimmed curved honeycomb panel with trim panel pinned to primary structure all along the transverse edges of the trim panel. There is 5% structural damping in the model.

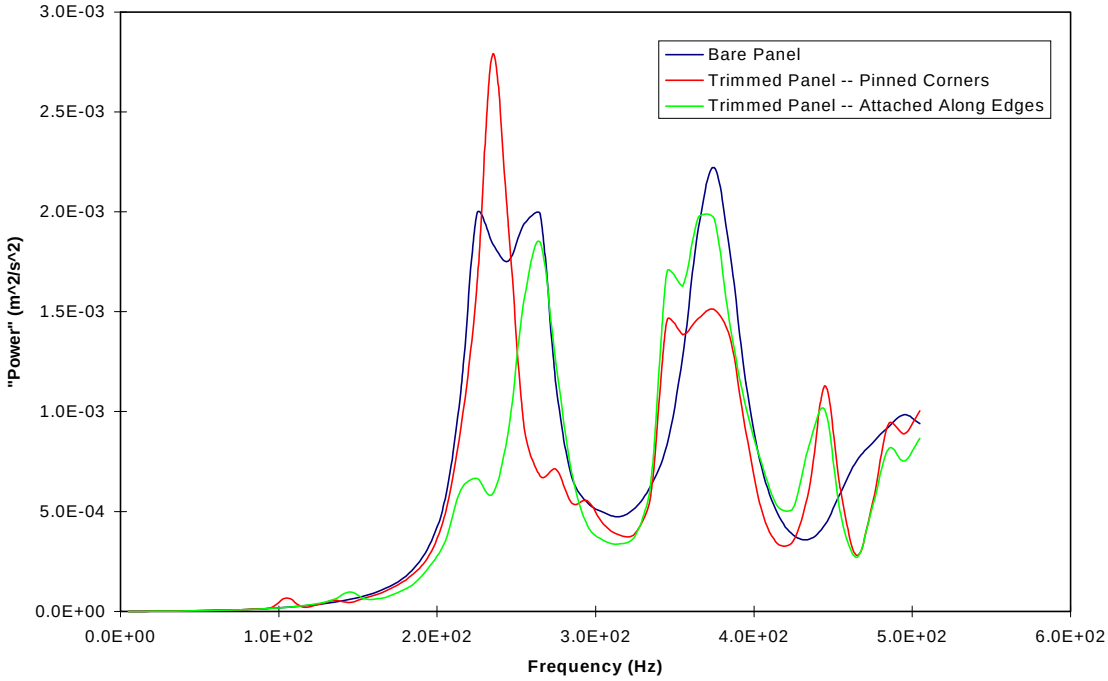

Figure 38 "Power" vs. Frequency for a grid point on the response side face sheet of the curved honeycomb panel. Node that in each of the three cases, a different grid point was used. There is 5% structural damping in the model.

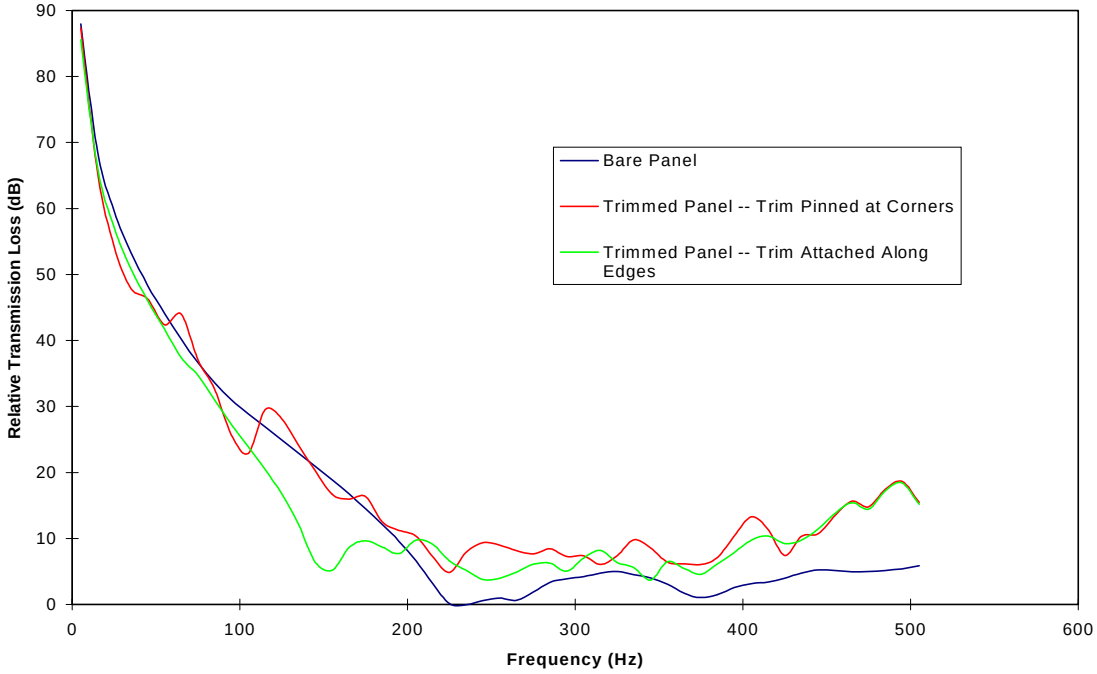

Figure 39 Relative Transmission Loss vs. Frequency for the curved honeycomb panel for the bare panel structure alone and both built-up configurations. There is 5% structural damping.

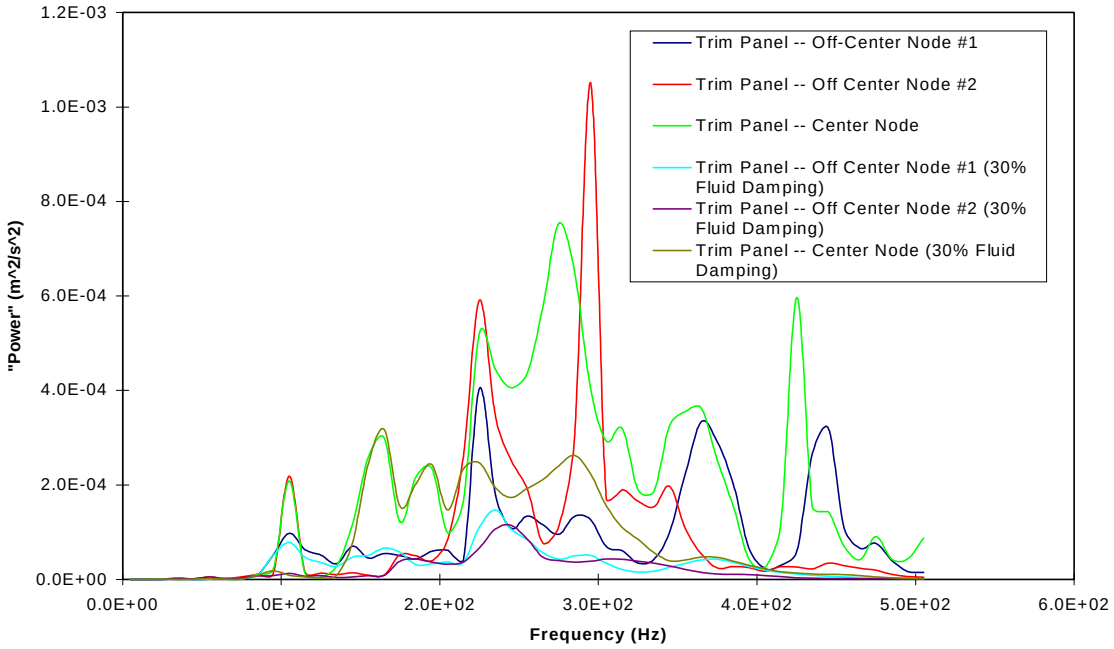

Figure 40 "Power" vs. Frequency for trimmed curved honeycomb panel with trim pinned to primary structure only at the trim panel corners. There is 5% structural damping in the model. This figure shows the same three curves as in Figure 35 and also contains the curves for the case in which there is 30% fluid damping in the air gaps between the primary structure and the trim panels.

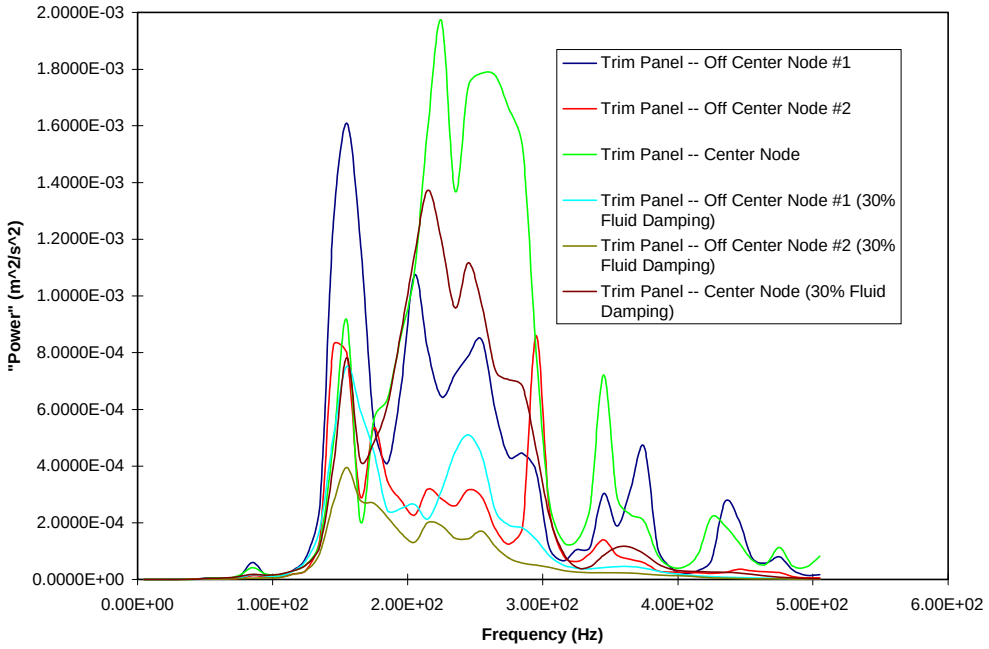

Figure 41 "Power" vs. Frequency for trimmed curved honeycomb panel with trim pinned to primary structure all along the transverse edges. There is 5% structural damping in the model. This figure shows the same three curves as in Figure 36 and also contains the curves for the case in which there is 30% fluid damping in the air gaps between the primary structure and the trim panels.

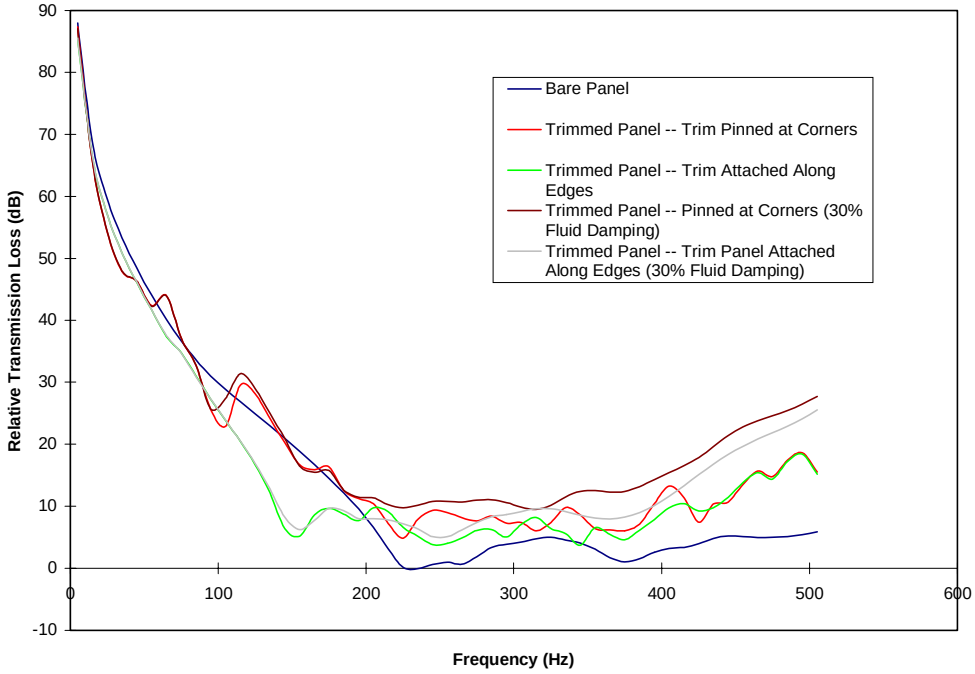

Figure 42 Relative Transmission Loss vs. Frequency for the curved honeycomb panel for the bare panel configuration and both trim panel mounting configurations. This figure contains the same three curves as in Figure 38 and also contains the curves for the case in which there is 30% fluid damping in the air gaps between the primary structure and the trim panels. There is 5% structural damping in all cases.

APPENDIX C – TABLES

Intrinsic Material Properties of Ti-3Al-2.5V	
Weight Density: ρ (N/m^3)	43992
Young's Modulus: E (GPa)	103.33
Shear Modulus: G (GPa)	43.752
Material Properties of Im7/Peti5 Layers	
Young's Modulus: E_{11} (GPa)	151.92
Young's Modulus: E_{22} (GPa)	9.646
Shear Modulus: G_{12} (GPa)	2.564
Poisson's Ratio: ν_{12}	0.34
Coefficient of Thermal Expansion: α_{11} (in/in/°F)	-1.9E-07
Coefficient of Thermal Expansion: α_{22} (in/in/°F)	1.55E-05
Weight Density: ρ (N/m^3)	15750
Ply Thickness: t (m)	1.397E-04

Table 1 Material Properties of Ti3Al2.5V and Im7/Peti5

Mode	Frequency
(1,1)	82.354
(1,2)	169.243
(2,1)	169.302
(2,2)	240.893
(3,1)	310.345
(1,3)	312.275
(3,2)	366.178
(2,3)	366.336
(3,3)	466.609

Table 2 Mode shapes and associated frequencies for the flat sandwich panel with isotropic core. The numbering of the mode shapes is based upon results generated by Leissa for a clamped, square, isotropic, plate. [12]

Titanium Honeycomb Core	
Weight Density: ρ (N/m^3)	1066.5
Young's Modulus*: $E_{11}=E_{22}$ (Pa)	1.65E+05
Young's Modulus: E_{33} (Pa)	1.03E+09
Shear Modulus: G_{13} (Pa)	4.82E+08
Shear Modulus: G_{23} (Pa)	4.82E+08
Shear Modulus*: G_{12} (Pa)	3.38E+08

Table 3 Equivalent Material Properties of Titanium Honeycomb Core partly based on formulation by Tang et al, and partly based on measured material properties (Properties marked with an asterisk denote those which were calculated from the intrinsic material properties).

Mode	Predicted Frequency (Hz)	Experimental Frequency (Hz)	Percent Difference (%)
(2,2)	147.2	132.3	11.3
(1,3)	209.3	200.3	4.5
(3,1)	268.9	241.3	11.4
(3,2)	365.2	331.6	10.1
(2,3)	367.0	336.6	9.0

Table 4 Mode shapes and associated frequencies for the flat sandwich panel with honeycomb core. The predicted frequencies are those calculated using MSC/NASTRAN. The experimental frequencies are those found from the experimental modal analysis. There is an average percent difference of 9.3% between the two sets of frequencies. The numbering of the mode shapes is based upon results generated by Leissa for a square, isotropic plate with free edges. [12]

Mode	Frequency
(1,1)	381.63

Table 5 Mode shape and associated frequency for the flat sandwich panel with honeycomb core. Note that all higher modes have frequencies beyond the frequency range of study. The numbering of this mode shape is based upon results generated by Leissa for a square, isotropic plate with clamped edges. [12]

Material Properties of the Aluminum 5052 Honeycomb Core	
Mass Density: ρ (kg/m^3)	91.2
Young's Modulus: E_{11} (GPa)	1.288
Young's Modulus: $E_{22}=E_{33}$ (MPa)	1.288
Shear Modulus: G_{23} (Kpa)	42.6
Shear Modulus: $G_{12}=G_{13}$ (KPa)	89.4
Poisson's Ratio: ν_{12}	0.40

Table 6 Material properties of Aluminum Honeycomb Core of Curved Panel. All of these properties for the core were measured. These properties are defined in a cylindrical coordinate system, which is shown in Figure 11 and Figure 12. The index '1' here refers to the radial, or out-of-plane, direction. The index '2' refers to the transverse direction, or the in-plane direction which runs along the curvature of the panel. The index '3' denotes the other in-plane direction which runs longitudinally along the panel.

Material Properties of BMS-8-212 Type III	
Mass Density: ρ (kg/m^3)	1550.3
Young's Modulus: E_{11} (GPa)	117.8
Young's Modulus: E_{22} (GPa)	8.819
Shear Modulus: $G_{12}=G_{23}=G_{13}$ (GPa)	4.616
Poisson's Ratio: ν_{12}	0.34
Coefficient of Thermal Expansion: α_{11} (m/m/°F)	0.02E-06
Coefficient of Thermal Expansion: α_{22} (m/m/°F)	15.0E-06
Ply Thickness: t (mm)	.1498
Material Properties of BMS-8-212 Type IV	
Mass Density: ρ (kg/m^3)	1522.6
Young's Modulus: $E_{11}=E_{22}$ (GPa)	57.19
Shear Modulus: $G_{12}=G_{23}=G_{13}$ (GPa)	4.616
Poisson's Ratio: ν_{12}	0.06
Coefficient of Thermal Expansion: $\alpha_{11=}\alpha_{22}$ (m/m/°F)	1.6E-06
Ply Thickness: t (mm)	.2108

Table 7 Material properties of BMS-8-212 Type III and Type IV (defined in the traditional cartesian coordinate system, where the index '3' denotes the out-of-plane direction).

Ply Number	Material	Orientation
1	BMS-8-212 Type III	45°
2	BMS-8-212 Type III	-45°
3	BMS-8-212 Type III	90°
4	BMS-8-212 Type III	0°
5	BMS-8-212 Type III	90°
6	BMS-8-212 Type III	-45°
7	BMS-8-212 Type III	45°
8	BMS-8-212 Type IV	0/90°

Table 8 Stacking sequence of the laminated composite face sheets for the curved honeycomb panel. Ply #1 is closest to the core and Ply #8 is the top ply, at the surface of the panel. The orientation angle is given relative to the positive 'z' direction in the cylindrical coordinate system defined in Figures 11 and 12.

Material Properties of Aluminum 2024 (used for flanges)	
Mass Density: ρ (kg/m^3)	2768.3
Young's Modulus: E (GPa)	73.03
Shear Modulus: G (GPa)	27.56
Coefficient of Thermal Expansion: α (m/m/°F)	12.9E-06
Material Properties of Aluminum 6061 (used for webs)	
Mass Density: ρ (kg/m^3)	2768.3
Young's Modulus: E (GPa)	68.90
Shear Modulus: G (GPa)	25.84
Coefficient of Thermal Expansion: α (m/m/°F)	13.0E-06

Table 9 Material properties for Aluminum 2024 and 6061, which comprise the stiffeners. Both materials are isotropic.

Mode	Predicted Frequency (Hz)	Experimental Frequency (Hz)	Percent Difference (%)
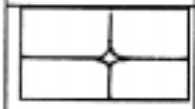	11.26	12.24	8.0
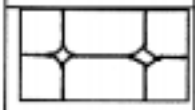	39.62	41.24	3.9
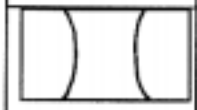	89.93	84.34	5.4
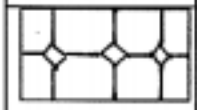	100.8	97.37	2.5
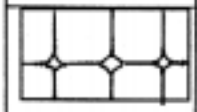	106.5	104.2	2.2
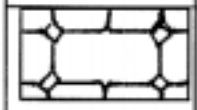	131.8	123.6	6.7
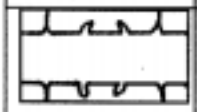	145.7	145.2	0.3

Table 10 Mode shapes and associated frequencies for the curved honeycomb panel in the free-free boundary condition configuration. Note that only the first seven modes are listed. This is due to the number of reference points in the experimental set-up. Only the first seven mode shapes could be accurately resolved given the number of reference points. There is an average percent difference of 4.1% between the predicted and experimental frequencies.

Mode	Frequency (Hz)
	226.6
	234.0
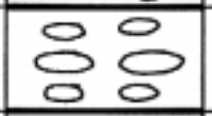	244.9
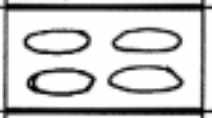	261.7
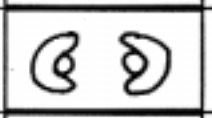	297.5
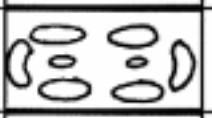	309.7
	335.0
	364.7
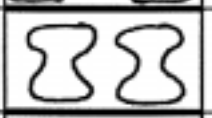	374.5
	408.8
	419.0
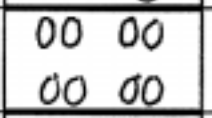	459.4
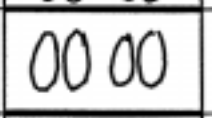	462.0
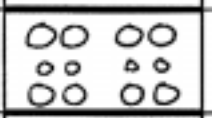	475.6
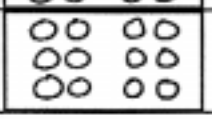	485.1

Table 11 Mode shapes and associated frequencies of the curved honeycomb panel with the edges clamped. Note that only significant panel modes have been included in this list. Modes which only have motion of the stiffeners are not included since they do not contribute as much to the radiated sound field.

Material Properties of Trim Panels	
Mass Density : ρ (kg/m^3)	1750.0
Young's Modulus: E (GPa)	26.1
Shear Modulus: G (GPa)	11.2
Thickness: t (mm)	1.30

Table 12 Material Properties for the cargo liner material which makes up the trim panels.

Appendix D – FORTRAN Codes

There were two main external FORTRAN codes written to perform calculations and manipulate results. The first of these is 'response.f'. This code was written to read the acoustic pressures calculated in the far-field spherical data recovery mesh in the COMET/Acoustics results file. It then uses these results to build the transfer matrix. It then performs the calculation $H_{mn}{}^{T}S_{ab}H_{mn}{}^{*}$, to calculate the power spectral density. Finally, the code uses this to calculate the transmission loss. There are three parameters in the source code which must be modified before compiling it. These are bcsets, nperset, and nnodes. These are the number of patches, the number of nodes per patch and the number of total nodes on the incident side of the panel respectively. The COMET/Acoustics results file must be in a file called 'results'. The transmission loss is written in a file called 'tranloss'.

The other code is called 'comet2nastran.f'. This code was used to read the elemental pressures on the boundary element mesh due to the oblique plane wave excitation form the COMET/Acoustics results file. It writes all the necessary MSC/NASTRAN bulk data cards to set up the excitation case in order to perform a frequency response analysis. These results are written to a number of different files, which are listed in the comments of the program. Note that this code is not robust by any means. It is written to write the appropriate bulk data cards for the particular boundary element mesh used for the curved honeycomb panel. It picks out only the elements in the mesh which correspond to the actual elements and the element identification numbers on

the incident side of the panel. For a different panel, mesh, or element numbering scheme, the source code will have to be significantly modified.

D.1 Response.f

```
PROGRAM response
ccccccccccccccccccccccccccccccccccccccccccccccccccccccccccccccccccccccccc
c                                                                       c
c   This program takes a COMET/Acoustics results file and writes        c
c   the magnitude and phase of the radiated acoustic pressure to        c
c   a transfer matrix.  This transfer matrix is then used along         c
c   with a cross-correlation matrix, which describes the                c
c   excitation, to determine the panel response by performing           c
c   the calculation:                                                    c
c                 T     *                                             c
c              [H] [S][H]                                               c
c                                                                       c
c   It then gives the radiated power for each frequency.                c
c   From the power, the transmission loss is calculated.                c
c   The program writes the power for each frequency in a file           c
c   called 'tranloss'.                                                  c
c                                                                       c
c   Written by Larry Barisciano,  August 1997                           c
c   Modified October 1997                                               c
c   Modified April 1998                                                 c
c   Modified June 1998                                                  c
c                                                                       c
ccccccccccccccccccccccccccccccccccccccccccccccccccccccccccccccccccccccccc
      implicit real*8(a-h,o-z)
      parameter(bcsets=9, nperset=25, drnodes=386, fr=51,nnodes=169)
      character*80 title,apm,app,spl,xvm,xvp,yvm,yvp,zvm,zvp
      character*80 magv,xi,yi,zi,descrp,end(2)
      character*80 freqinfo(3)
      character*80 header(3)
      character*20 junk1
      character*80 headers(3),junk(3),junk2
      character*21 analid,numnod,vpernod,record
      character*10 node
      complex pressure(bcsets,drnodes,fr)
      complex conj(bcsets,drnodes,fr)
      complex trans(drnodes,bcsets,fr), power(fr)
      complex resp(drnodes,drnodes,fr)
      complex prod(drnodes, bcsets,fr)
      real exc(bcsets,bcsets), rho, c, radius, integ
      integer nodnum,anals,freqs
      integer freq1,acquans
      real freq(fr),imag,real,rad,hz,pow1,pow2,tranloss
      real input
      open(unit=10,file='results',status='old')
      open(unit=11,file='panel_response',status='unknown')
      open(unit=12,file='tranloss',status='unknown')
      read(10,74) title
```

```
read(10,74) junk2
read(10,25) junk1,anals
rho=1.21
c=343.0
acquans=2
radius=87.0
integ=(4*3.14*radius**2)/drnodes
freqs=int(anals/bcsets)
do i=1,3
        read(10,74) header(i)
enddo
do ii=1,anals
   do j=1,3
         read(10,74) freqinfo(j)
   enddo
   read(10,50) freq(ii)
enddo
do i=1,3
   read(10,74) junk(i)
enddo
do k=1,bcsets
   do m=1,freqs
      do l=1,3
         read(10,74) headers(l)
      enddo
      read(10,74) analid
           read(10,74) numnod
           read(10,74) vpernod
      read(10,74) record
      read(10,74) descrp
           read(10,74) spl
      read(10,74) apm
      read(10,74) app
      read(10,74) xvm
      read(10,74) xvp
      read(10,74) yvm
      read(10,74) yvp
      read(10,74) zvm
      read(10,74) zvp
      read(10,74) magv
      read(10,74) xi
      read(10,74) yi
      read(10,74) zi
      do n=1,drnodes
         read (10,80) node,nodnum
         read (10,90) spl1,apm1,app1,xvm1,xvp1,yvm1
         read (10,90) yvp1,zvm1,zvp1,magv1,xi1,yi1
         read (10,110) zi1
         rad=(app1*3.14159)/180
                  real=apm1*cos(rad)
         imag=apm1*sin(rad)
         pressure(k,n,m)=cmplx(real,imag)
         conj(k,n,m)=conjg(pressure(k,n,m))
         trans(n,k,m)=pressure(k,n,m)
      enddo
```

```
            do nn=1,2
               read(10,74) end(nn)
            enddo
          enddo
        enddo
        do i=1,bcsets
          do j=1,bcsets
            if (i .eq. j) then
              exc(i,j)=1.0
            else
              exc(i,j)=0.0
            endif
          enddo
        enddo
        do k=1,freqs
          power(k)=(0.0,0.0)
          do i=1,drnodes
            do j=1,bcsets
              prod(i,j,k)=(0.0,0.0)
              do n=1,bcsets
                prod(i,j,k)=prod(i,j,k)+trans(i,n,k)*exc(n,j)
              enddo
            enddo
          enddo
          do i=1,drnodes
            do j=1,drnodes
              resp(i,j,k)=(0.0,0.0)
              do n=1,bcsets
                resp(i,j,k)=resp(i,j,k)+prod(i,n,k)*conj(n,j,k)
              enddo
            enddo
          enddo
          do iii=1,drnodes
            power(k)=power(k)+((0.5*integ*resp(iii,iii,k))/(rho*c))
          enddo
          write(11,180) freq(k),power(k)
        enddo
        close(11)
        input=(bcsets*nperset**2)/(nnodes)**2
        open(unit=11,file='panel_response',status='old')
        write(12,185)
        do i=1,freqs
              read(11,180) hz,pow1,pow2
          tranloss=10*alog10(input/pow1)
          write(12,190) hz,pow1,tranloss
        enddo
ccccccccccccccccccccccccccccccccc
c     FORMAT STATEMENTS        c
ccccccccccccccccccccccccccccccccc
 25    format(a20,i3)
 50    format(1x,e11.5)
 60    format(f2.1)
 74    format(a80)
 80    format(a13,i5)
 90    format(6(2x,e11.5))
```

```
 110   format(2x,e11.5)
 130   format(e11.5)
 140   format(e11.5,1x,e11.5)
 180   format(f5.1,1x,e11.5,1x,e11.5)
 185   format('Freq      Power      Tranloss')
 190   format(f5.1,1x,e11.5,1x,f11.5)
       close(10)
       close(11)
       close(12)
       end
```

D.2 Comet2nastran.f

```
PROGRAM comet2nastran
ccccccccccccccccccccccccccccccccccccccccccccccccccccccccccccccccccccc
c                                                                     c
c   This program takes a COMET/Acoustics element results             c
c   file and writes the magnitude and phase of the pressure           c
c   for each element in a format usable by MSC/NASTRAN.               c
c   Specifically, it converts the magnitude and phase of the          c
c   pressure to the real and imaginary parts and then writes          c
c   the values as TABLED1 entries to the file 'tables' for            c
c   use in the NASTRAN bulk data file                                 c
c   The program also writes the RLOAD1,LSEQ,DLOAD and PLOAD4c
c   bulk data cards.  These cards are written to the two              c
c   files 'dload' and 'pload'                                         c
c   This program has been specifically written for the case           c
c   of a plane wave impinging on a curved panel.  Thus it             c
c   only writes the pressures for the elements of the BEM             c
c   which correspond to elements of the specific curved panel         c
c   of interest.  The parameters in the code must be                  c
c   appropriately adjusted to apply this to a different panel.        c
c                                                                     c
c   Written by Larry Barisciano  June 1998                            c
c                                                                      c
ccccccccccccccccccccccccccccccccccccccccccccccccccccccccccccccccccccc
      implicit real*8(a-h,o-z)
      parameter (fr=51,loadset=2642)
      parameter (link=1586)
      character*80 title,apm,app,spl,nvm,nvp,nai,nri
      character*80 descrp,end(2)
      character*80 freqinfo(3), header(3)
      character*20 junk1
      character*80 headers(3),junk(3),junk2
      character*21 analid,vperelm,record
      character*12 elm
      character*19 number
      character*8 z1,z2,z3
      character*1 s1,s2,s3,s4
      complex pres(51,2000),conj(51,2000),totpres(51)
      complex ppstar
      real slp1,apm1,app1,nvm1,nvp1,nai1,nri1
```

```
      integer elmnum,anals,tabid,rloadid,dloadid
      integer freq1,numelm,rloadid2,rloadid3,rloadid4
      integer tab1,tab2,rl,lin,eid
      real f(fr),s(51,2000),r(51,2000),rho,c,integ
      open(unit=10,file='results',status='old')
      open(unit=11,file='tables',status='unknown')
      open(unit=12,file='dload',status='unknown')
      open(unit=13,file='pload',status='unknown')
      rloadid=1585
      dloadid=2641
      read(10,74) title
      read(10,74) junk2
      read(10,25) junk1,anals
      do i=1,3
        read(10,74) header(i)
      enddo
      do ii=1,anals
        do j=1,3
          read(10,74) freqinfo(j)
        enddo
        read(10,50) f(ii)
      enddo
      do i=1,3
        read(10,74) junk(i)
      enddo
      do m=1,anals
        do l=1,3
          read(10,74) headers(l)
        enddo
        read(10,74) analid
        read(10,98) number,numelm
        read(10,74) vperelm
        read(10,74) record
        read(10,74) descrp
        read(10,74) spl
        read(10,74) apm
        read(10,74) app
        read(10,74) nvm
        read(10,74) nvp
        read(10,74) nai
        read(10,74) nri
        do n=1,numelm
          read(10,80) elm,elmnum
          read(10,*) spl1,apm1,app1,nvm1,nvp1,nai1
          read(10,110) nri1
          if (elmnum.gt.1056) then
            goto 63
          endif
          rad=(app1*3.14159)/180
          r(m,elmnum)=apm1*cos(rad)
          s(m,elmnum)=apm1*sin(rad)
63      enddo
        do nn=1,2
          read(10,74) end(nn)
        enddo
```

```
 enddo
 numtabs=fr/4+1
 s1=' '
 s2=' '
 s3='A'
 s4=' '
 tabid=1
 j=1
 z1='TABLED1 '
 z2='+     R0'
 write(11,120) z1,tabid,z2
 z1=z2
 z2='+     R1'
 i0=ichar(s3)
 i=0
 ii=0
 iii=0
 iiii=0
 do kkk=1,676
   call findz2(i0,i,ii,iii,iiii,s1,s2,s3,s4,z3)
 enddo
 do ll=529,1056
   do mm=1,2
     do kk=1,numtabs
       m=j+1
       n=j+2
       k=j+3
       if ((mm.eq.1).and.(kk.ne.13)) then
         write(11,130)z1,f(j),r(j,ll),f(m),r(m,ll),f(n)
& ,r(n,ll),f(k),r(k,ll),z2
       endif
       if ((mm.eq.1).and.(kk.eq.13)) then
         write(11,132)z1,f(j),r(j,ll),f(m),r(m,ll),f(n)
3 ,r(n,ll)
       endif
       if ((mm.eq.2).and.(kk.ne.13)) then
         write(11,130)z1,f(j),s(j,ll),f(m),s(m,ll),f(n)
4 ,s(n,ll),f(k),s(k,ll),z2
       endif
       if ((mm.eq.2).and.(kk.eq.13)) then
         write(11,132)z1,f(j),s(j,ll),f(m),s(m,ll),f(n)
5 ,s(n,ll)
       endif
       z1=z2
       j=j+4
       call findz2(i0,i,ii,iii,iiii,s1,s2,s3,s4,z2)
     enddo
     tabid=tabid+1
     j=1
     z1='TABLED1 '
     write(11,120) z1,tabid,z2
     z1=z2
     call findz2(i0,i,ii,iii,iiii,s1,s2,s3,s4,z2)
   enddo
 enddo
```

```
      tab1=1
      tab2=2
      rl=rloadid
      lin=link
      do no=1,numelm
        write(12,30) rl,lin,tab1,tab2
        write(12,40) loadset,lin,tabid
        rl=rl+2
        lin=lin+2
        tabid=tabid+1
        tab1=tab1+2
        tab2=tab2+2
      enddo
      lin=lin-2
      rloadid2=rloadid+2
      rloadid3=rloadid+4
      rloadid4=rloadid+6
      z1='DLOAD   '
      write(12,44)z1,dloadid,rloadid,rloadid2,rloadid3,z2
      z1=z2
      call findz2(i0,i,ii,iii,iiii,s1,s2,s3,s4,z2)
      do jkl=rloadid4,lin,8
        jkl1=jkl+2
        jkl2=jkl+4
        jkl3=jkl+6
        write(12,45)z1,jkl,jkl1,jkl2,jkl3,z2
        z1=z2
        call findz2(i0,i,ii,iii,iiii,s1,s2,s3,s4,z2)
      enddo
      eid=529
      do lmn=1057,1584
        write(13,140)lmn,eid
        eid=eid+1
      enddo
ccccccccccccccccccccccccccccccccc
c     FORMAT STATEMENTS          c
ccccccccccccccccccccccccccccccccc
 25   format(a20,i3)
 30   format('RLOAD1  ',i4,4x,i4,4x,16x,i8,i8)
 40   format('LSEQ    ',i4,4x,i4,4x,i4)
 44   format(a8,i4,4x,'1.',6x,3('1.',6x,i4,4x),a8)
 45   format(a8,4('1.',6x,i4,4x),a8)
 50   format(1x,e11.5)
 74   format(a80)
 80   format(a12,i4)
 90   format(6(1x,e11.5))
 98   format(a19,i4)
 110   format(2x,e11.5)
 120   format(a8,i8,56x,a8)
 130   format(a8,4(f8.1,f8.4),a8)
 132   format(a8,3(f8.1,f8.4),4x,'ENDT')
 140   format('PLOAD4  ',i8,i8,6x,'1.')
      close(10)
      close(11)
      close(12)
```

```
close(13)
end
subroutine findz2(i0,i,ii,iii,iiii,s1,s2,s3,s4,z2)
character*8 z2
character*1 s1,s2,s3,s4
if(i.lt.25)then
  i=i+1
  s3=char(i0+i)
  else
  i=0
  ii=ii+1
  if (ii.lt.25) then
    s3='0'
    s4=char(i0+ii-1)
    else
    ii=0
    iii=iii+1
    if (iii.lt.25) then
      s3='0'
      s4='0'
      s2=char(i0+iii-1)
      else
      iii=0
      iiii=iiii+1
      s3='0'
      s4='0'
      s2='0'
      s1=char(i0+iiii-1)
    endif
  endif
endif
z2='+   '//s1//s2//s4//s3
end
```

REPORT DOCUMENTATION PAGE

Form Approved
OMB No. 0704-0188

1. AGENCY USE ONLY (*Leave blank*)	2. REPORT DATE	3. REPORT TYPE AND DATES COVERED
	November 1999	Contractor Report

4. TITLE AND SUBTITLE
Broadband Transmission Loss Due to Reverberant Excitation

5. FUNDING NUMBERS
C NCC1-14
WU 537-06-37-20

6. AUTHOR(S)
Lawrence P. Barisciano, Jr.

7. PERFORMING ORGANIZATION NAME(S) AND ADDRESS(ES)
The George Washington University
Joint Institute for the Advancement of Flight Sciences
c/o NASA Langley Research Center
Hampton, VA 23681-2199

8. PERFORMING ORGANIZATION REPORT NUMBER

9. SPONSORING/MONITORING AGENCY NAME(S) AND ADDRESS(ES)
National Aeronautics and Space Administration
Langley Research Center
Hampton, VA 23681-2199

10. SPONSORING/MONITORING AGENCY REPORT NUMBER
NASA/CR-1999-209687

11. SUPPLEMENTARY NOTES
Final Report
Technical Monitor: Richard J. Silcox

12a. DISTRIBUTION/AVAILABILITY STATEMENT
Unclassified-Unlimited
Subject Category 71 Distribution: Nonstandard
Availability: NASA CASI (301) 621-0390

12b. DISTRIBUTION CODE

13. ABSTRACT *(Maximum 200 words)*
The noise transmission characteristics of candidate curved aircraft sidewall panel constructions is examined analytically using finite element models of the selected panel geometries. The models are validated by experimental modal analyses and transmission loss testing. The structural and acoustic response of the models are then examined when subjected to random or reverberant excitation, the simulation of which is also discussed. For a candidate curved honeycomb panel, the effect of add-on trim panel treatments is examined. Specifically, two different mounting configurations are discussed and their effect on the transmission loss of the panel is presented. This study finds that the add-on acoustical treatments do improve on the primary structures transmission loss characteristics, however, much more research is necessary to draw any valid conclusions about the optimal configuration for the maximum noise transmission loss. This paper describes several directions for the extension of this work.

14. SUBJECT TERMS
Aircraft interior noise; Noise transmission; Finite element modeling; Aircraft sidewalls

15. NUMBER OF PAGES
102

16. PRICE CODE
A06

17. SECURITY CLASSIFICATION OF REPORT	18. SECURITY CLASSIFICATION OF THIS PAGE	19. SECURITY CLASSIFICATION OF ABSTRACT	20. LIMITATION OF ABSTRACT
Unclassified	Unclassified	Unclassified	UL